Accepted Manuscript

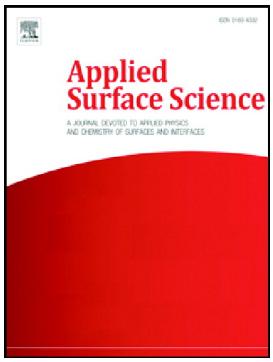

Short and long term surface chemistry and wetting behaviour of stainless steel with 1D and 2D periodic structures induced by bursts of femtosecond laser pulses

Giuseppe Giannuzzi, Caterina Gaudiuso, Rosa Di Mundo, Luciana Mirenghi, Fotis Fraggelakis, Rainer Kling, Pietro Mario Lugarà, Antonio Ancona

PII: S0169-4332(19)32162-2
DOI: https://doi.org/10.1016/j.apsusc.2019.07.126
Reference: APSUSC 43384

To appear in: *Applied Surface Science*

Received date: 28 May 2019
Revised date: 12 July 2019
Accepted date: 15 July 2019

Please cite this article as: G. Giannuzzi, C. Gaudiuso, R. Di Mundo, et al., Short and long term surface chemistry and wetting behaviour of stainless steel with 1D and 2D periodic structures induced by bursts of femtosecond laser pulses, Applied Surface Science, https://doi.org/10.1016/j.apsusc.2019.07.126

Short and long term surface chemistry and wetting behaviour of stainless steel with 1D and 2D periodic structures induced by bursts of femtosecond laser pulses

Giuseppe Giannuzzi[a], Caterina Gaudiuso[a,b,*], Rosa Di Mundo[c,**], Luciana Mirenghi[d], Fotis Fraggelakis[e,f], Rainer Kling[e], Pietro Mario Lugarà[a,b], Antonio Ancona[b]

[a] Dipartimento Interateneo di Fisica, Università degli Studi di Bari, Bari, Italy
[b] CNR-IFN UOS BARI, Via Amendola 173, Bari, Italy
[c] Dipartimento di Ingegneria Civile, Ambientale, del Territorio, Edile e di Chimica (DICATECh), Politecnico di Bari, via Orabona 4, 70126 Bari, Italy
[d] Agenzia nazionale per le nuove tecnologie, l'energia e lo sviluppo economico sostenibile (ENEA), Centro Ricerche Brindisi, via Appia km 706, 72100 Brindisi, Italy
[e] ALPhANOV, Technological Centre for Optics and Lasers, Rue F. Mitterrand, 33400 Talence, France
[f] Université de Bordeaux, CNRS, CEA, CELIA, UMR5107, 33405 Talence, France

*Corresponding author
E-mail: caterina.gaudiuso@uniba.it

Full postal address: Università degli Studi di Bari, Dipartimento Interuniversitario di Fisica, via Amendola 173, I-70126 Bari, Italy

**Corresponding author
E-mail: rosa.dimundo@poliba.it

Full postal address: Dipartimento di Ingegneria Civile, Ambientale, del Territorio, Edile e di Chimica (DICATECh), Politecnico di Bari, via Orabona 4, 70126 Bari, Italy

Abstract

We investigate the short and long term wettability of laser textured stainless steel samples in order to better understand the interplay between surface topography and chemistry. Very different 1D and 2D periodic as well as non-periodic surface patterns were produced by exploiting the extreme flexibility of a setup consisting of five rotating birefringent crystals, which allows generating bursts of up to 32 femtosecond laser pulses with fixed intra-burst delay of 1.5 ps. The change of the surface morphology as a function of the pulse splitting, the burst polarization state and the fluence was systematically studied. The surface topography was characterized by SEM and AFM microscopy. The laser textured samples exhibited, initially, superhydrophilic behaviour which, during exposure to ambient air, turned into superhydrophobic with an exponential growth of the static contact angle. The dynamic contact angle measurements revealed a water adhesive character which was explained by XPS analyses of the surfaces that showed an increase of hydrocarbons and more oxidized metal species with the aging. The characteristic water adhesiveness and superhydrophobicity of laser textured surfaces can be exploited for no loss droplet reversible transportation or harvesting.

Highlights

- 1D-LIPSS with variable period were obtained with bursts of linearly polarized pulses with ps intraburst delay
- 2D-LIPSS (triangles arranged over hexagons) were produced with bursts of crossed and circular polarization
- Changing the number of pulses within the bursts allowed varying the morphology of surface structuring among several patterns
- The contact angle of the laser treated surfaces varied over the time, settling at values close to 160° at long term with high hysteresis

- Over the exposure time the laser treated steel surfaces become richer in hydrocarbons and present more oxidized metals

Keywords: Laser structuring, LIPSS, Femtosecond lasers, Bursts, Metals, Wettability

1. Introduction

Laser-induced periodic surface structures (LIPSS) [1] are distinguished, depending to their spatial periodicity Λ, into low spatial frequency LIPSS (LSFL) that have Λ close to the laser wavelength, and high spatial frequency LIPSS (HSFL), which are characterized by a much smaller period, i.e. $\Lambda<\lambda/2$ [2]. Even though a complete theory to describe their formation has not been developed yet, LSFL generation on metals and semiconductors is mainly ascribed to interference effects between the laser induced surface plasmon polariton and the incident radiation, leading to localized power distribution and maxima of the electric field where ablation occurs, thus generating regular surface patterns. On the other hand, the formation of HSFL is attributed to the auto-arrangement of the roughness centers in periodic structures due to coherent superposition of the scattered waves produced by the near-field enhancements localized on the initial surface nano-roughness [3].
Recently it has been proposed that convection flow may occur during the melting of the surface and determine the HSFL formation [4].
LIPSS can be duly exploited to functionalize the surface of a huge variety of materials, such as metals [5,6], semiconductors [7,8] and dielectrics [9,10], for several application fields. In bioengineering and biomedicine, for example, LIPSS-covered surfaces are employed as anti-bacterial since the LIPSS morphology may inhibit bacteria adhesion [11] or, conversely, they can favour cell proliferation [12]. Texturing based on LIPSS has been demonstrated to be beneficial for reducing friction, thus enhancing the tribological performances of mechanical components [13]. LIPSS enable to change also the optical properties of a surface. Therefore, its absorptivity or reflectivity [14] or colour [15], can be conveniently modified with interesting applications in the field of sensors, decoration and anti-counterfeiting.
Another property that LIPSS can convey to a surface is a significant change of its wettability. Surfaces of different materials have shown hydrophobic or superhydrophobic behaviour after being laser textured with LIPSS [16–18]. This result is preliminary to the development of water repellent or even self-cleaning or anti-icing surfaces without employing any chemical treatment, which can find many applications in the aerospace and appliance industry. The hydrophobic behaviour of the laser textured surfaces has been mainly attributed to their morphological characteristics. Therefore, it is believed that by artificially reproducing on a surface the same micro- and nanoscale features observed in nature, for example, on a Lotus leaf is enough to convey to that surface the same superhydrophobic or self-cleaning properties.
Following this approach, many studies have recently investigated the relationship between the laser irradiation conditions and the morphology of the produced surface patterns aiming to control their geometrical features by simply tuning the laser parameters. On metals and semiconductors it was found that 1D-LIPSS consisting of parallel ripples are produced by irradiating the surface with linearly polarized laser pulses and that it is possible to control the orientation of the ripples by rotating the polarization axis of the incident light [19], while the spatial period and depth of the ripples can be tuned by changing the laser wavelength [20,21], the angle of incidence of the laser beam [22], the pulse-to-pulse spatial overlap [23,24], the fluence [25] and the ambient pressure [26]. Recently, it was reported that using bursts of linearly and parallel polarized pulses with picoseconds intra-burst delay it is possible to finely tune the LIPSS spatial period and depth by varying the intra-burst delay and the number of sub-pulses in the bursts [27].
Generation of 2D-LIPSS, i.e. surface patterns characterized by periodicity along two or more directions like e.g. square or triangular structures, have been demonstrated by several authors using circularly polarized laser pulses or crossed polarized double pulses with time delays in the picoseconds range [28–31]. The possibility of using bursts with more than two pulses with mixed polarizations to produce new morphologies of 2D LIPSS was not further explored. In this case, the pulse-to-pulse delay and the total burst duration to be investigated should be short enough to ensure that the occurrence of decomposition and melting of the lattice after energy absorption does not hinder the LIPSS formation.

However, it has been recently found that it is not only the surface topography that is responsible for the wetting behaviour of a laser-textured surface. Indeed, several works have shown that immediately after the laser treatment such surfaces exhibit hydrophilicity which turns into hydrophobicity after low temperature annealing [32] or after storage in ambient atmosphere as well as in polyethylene bags for a few weeks [18,33]. Therefore, besides the morphological features, a yet not fully understood surface chemistry effect must be taken into account. Most of the works that have tried to address this issue, have been limited to chemical composition measurements. Very few works have duly investigated the chemical bonds on the surface originating from the laser structuring and their time evolution. Rung et al. performed XPS measurements on both untreated and surface textured brass samples immediately after the laser irradiation and several days later. They found, especially for carbon and oxygen, changes in element concentration and binding conditions originated by the laser treatment. However, no significant evolution of the surface chemistry was found over the following days to justify the observed change of the wetting behaviour [32].
In this research study, two different aspects of the laser surface structuring process changing the wettability of steels samples have been investigated. The first part of the work is focused on the use of bursts of ps-delayed ultrashort laser pulses to produce LIPSS of different morphologies. In particular, burst with a varying number of pulses from 2 to 32 having time duration of 200 fs were employed with different polarization states, i.e. linearly polarized, circularly polarized and cross polarized. LIPSS generated in Normal Pulse Mode (NPM) are also reported for comparison. The surface topographies of the produced samples have been characterized by SEM and AFM microscopy. In the second part of the work, the wetting behaviour of the surfaces and its time evolution has been analyzed by static as well as dynamic contact angles measurements. Finally, accurate XPS measurements were carried out to assess the short and long term surface chemistry in relation to the wettability properties.

2. Experimental

2.1 Materials

The AISI type 301 stainless steel was used as substrate, known for its high corrosion resistance and high ductility, and subjected to the laser treatment just after the removal of the plastic protective film, without any type of cleaning procedure.

2.2 Burst generation and LIPSS formation

Figure 1 shows a sketch of the experimental setup employed in this work. A PHAROS laser system from Light Conversion emitting linearly polarized 200-fs (FWHM) pulses at a wavelength of 1030 nm with Gaussian energy distribution ($M^2 \sim 1.3$) was used for our experiments. The laser beam passed through a flexible and robust burst generator which produced a single burst from each incoming ultrafast laser pulse by means of an array of five calcite birefringent crystals [34,35]. According to the orientation of the optical axis of each crystal with respect to the polarization direction of the incident pulse [35], the latter was split into *n* sub-pulses (with n from 2 to 32) with equally fractioned energy. The intra-burst time delay Δt also depended on the orientation of the crystals and could take the following discrete values: 1.5 ps, 3 ps, 6 ps, 12 ps, and 24 ps. Typically, the sub-pulses emerging from the crystal array are alternately crossed-polarized, since half of them are parallel and half orthogonal to the optical axes of the crystals (Fig. 1a). In this case, the polarization state of the burst was indicated as XP, i.e. cross polarized burst. When a polarizer was placed after the optical chain of the calcite crystals, the XP burst was converted into linearly polarized (LP) burst (Fig. 1b). When placing instead a quarter-wave plate the burst polarization was modified into circularly polarized (CP) burst (Fig. 1c). The total energy per burst and/or the sub-pulses energy was finely adjusted by means of a half-wave plate and a polarizer placed upstream of the calcite crystals. A further half-wave plate was positioned after the burst generator to rotate the sub-pulse polarization at desired angles.
A galvo-scanner (SCANLAB's intelliSCAN 14) equipped with a F-Theta telecentric lens (56 mm of focal length) was used to move the laser beam over the stainless steel (AISI 301) polished

samples positioned on a 3-axis stage in the beam focal plane. The focused spot size on the sample surface *d* was 24 µm ± 1 µm (1/e2 peak intensity), measured with a CCD camera (FireWire BeamPro Model 2523 by Photon Inc.).

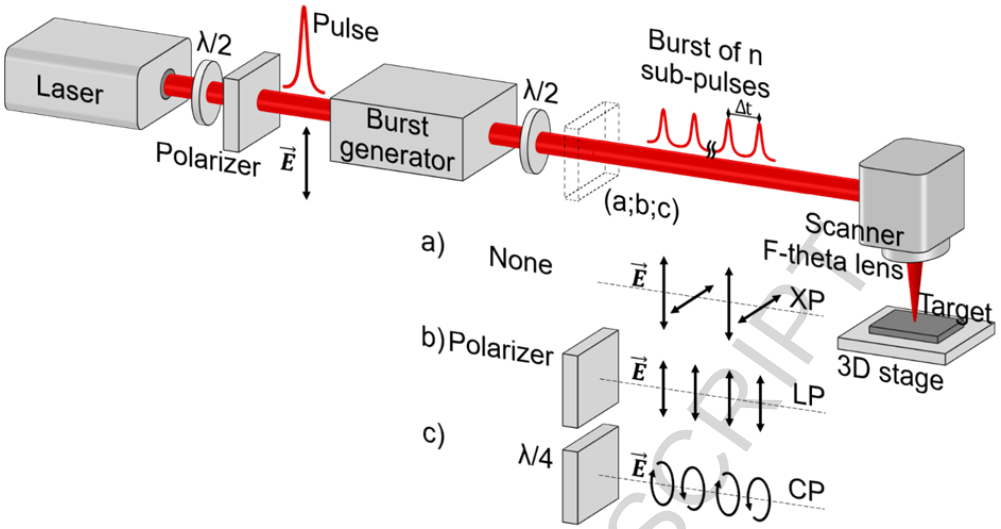

Fig. 1 - Sketch of the experimental setup used for the generation of the bursts and for the irradiation of the stainless-steel samples. The burst of n sub-pulses generated by burst generator were crossed-polarized (XP) as shown in (a). When a polarizer (b) or a quarter-wave plate (c) were placed into the beam line, the XP bursts were converted into linearly polarized (LP) or in circularly polarized (CP) bursts, respectively.

The scanning strategy to texture the samples surface consisted in scanning a regular pattern of successive parallel lines separated by a distance called hatch (h). Thus, the number of overlapped spot along the direction orthogonal to the scan line is given by d/h. The scanning speed v and the laser repetition rate f defined the average number of pulses irradiated on a dimensionless spot of the surface along a line scan, most commonly called “pulses per spot” (pps), calculated as pps=d*f/v [36]. Therefore, the total number of overlapped pulses (pps_{tot}) can be calculated as (d/h)*pps and determines the total actual fluence impinging on the sample surface, which is given by the fluence of the single pulse multiplied by pps_{tot}.
The laser repetition rate was fixed at 200 kHz to ensure processing speeds high enough. Relatively large textured area of about 200 mm^2 were produced to investigate the wettability properties. All experiments have been performed in ambient air.

2.3 Surface characterization

After laser irradiation, the morphology of the surface structures was characterized using a scanning electron microscope (SEM, Carl Zeiss mod. Σigma) and an atomic force microscope (AFM, NT-MDT mod. Ntegra). The acquired SEM images were processed by Gwyddion software by means of the Fourier transform (FT), to determine the spatial period of the laser-induced structures.
In order to highlight the influence of the laser treatment on the surface wettability, a digital goniometer, consisting of a Dino-lite portable microscope combined with a cold light lamp for back-lighting of the drop, was employed to capture the water drop images and videos for measuring, respectively, the static and the dynamic water contact angle (WCA). Static measurements were performed on selected samples by dispensing 5 µL drops of bi-distilled water onto the samples surface. In order to investigate the aging effect on the sample wetting properties, WCA measurements were firstly performed at time “zero” (within one day from the laser treatment), and then repeated every week for 7 weeks on the same samples stored in ambient air, until a steady-state wetting behaviour was observed.
Advancing and receding (dynamic) angles were measured only on the untreated-and unpolished-sample and on the laser-treated aged samples (i.e. at steady state, after two months) with the sessile drop technique. It consists in inducing variations of the drop volume, from 1 to 5 µL, at a

speed of 0.5 µL /s, on the sample. Advancing angles are the maximum angles observed during the droplet growth, while receding angles are the ones just before observation of the contact surface reduction. Each WCA value has been obtained by averaging four measurements.
Surface sensitive analyses were performed with X-ray Photoelectron Spectroscopy (XPS) by using a Versa Probe 5000 PHI Spectrometer equipped with a monochromatic Al-X Ray source at low power and a hemispherical analyzer in the Fixed Analyser Transmission (FAT) mode. A take-off angle of 90° was utilised. Surface scans were performed in different regions of the samples using the mono X-ray source at a power of 25 W and an acceleration voltage of 15kV, with a spot size of 100µm. Survey scans were recorded for all the samples in the range of 0-1400 eV of binding energy, with a pass energy of 187.85 eV. Narrow scan high resolution spectra of C1s, O1, Fe2p and Cr2p were acquired with a pass energy of 50 eV.
Best fitting of the C 1s XPS line shape has been performed by means of the casaXPS software.

3. Results and discussion

3.1 Surface structuring with linearly and circularly polarized normal pulses

In Figure 2, the different morphologies obtained in NPM with linear and circular polarization are shown as a function of the applied fluence.

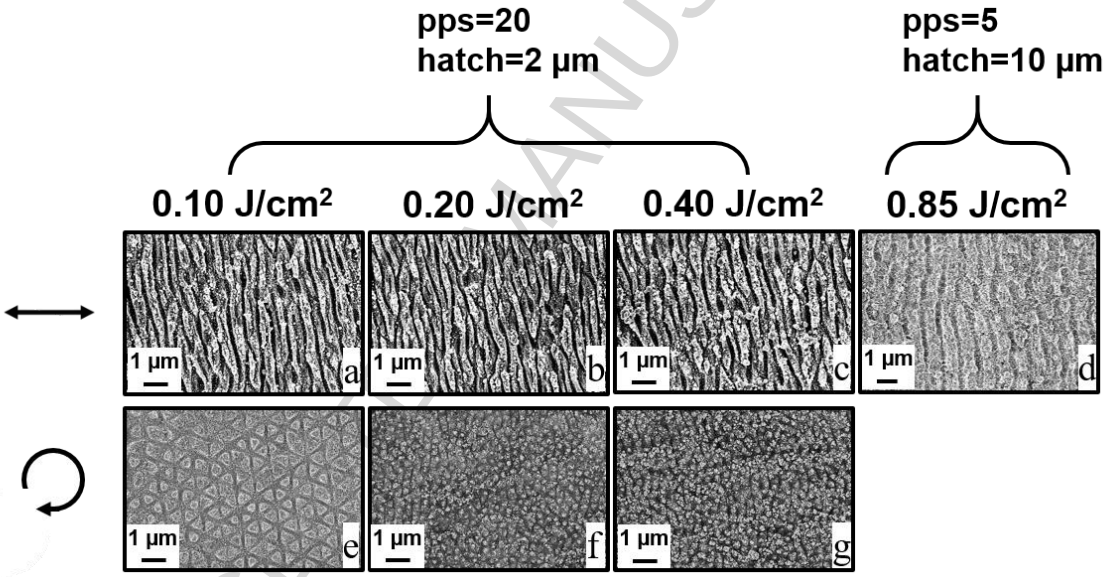

Fig. 2 – Different morphologies obtained in NPM with linear (a)-(d) and circular (e)-(g) polarization and different pulse fluence values.

As long as the accumulated fluence is higher than or equal to 24 J/cm^2, linear polarization leads to the formation of HSFL presenting bifurcations and interruptions. On the other hand, a lower accumulated fluence allows the generation of LSFL with a spatial period of 902 ± 1 nm.
With the change into circular polarization, slight triangular structures arranged in hexagonal patterns are obtained, but only with pps_{tot}=240 each at 0.10 J/cm^2. Similar structures have been reported in literature for analogous irradiation conditions [37]. At higher fluences, the triangular patterns are replaced by disordered pillar-like structures.

3.2 Surface structuring with parallel linearly polarized bursts

In Figure 3, we report the SEM images of LIPSS obtained with bursts having an intra-burst delay of 1.5 ps and a variable number of pulses having horizontal polarization. Analogous surface obtained under NPM irradiation is also shown for comparison. Interestingly, the structures obtained in BM have similar features to those reported in NPM: they are 1D-LSFL with a spatial period close to the laser wavelength and an orientation perpendicular to the incident polarization. It is worth noticing

that the periodic surface structures become slightly less uniform as *n* increases, owing to the occurrence of several interruptions and/or bifurcations. More accurate acquisitions of the 3D profiles by AFM allowed precisely measuring the depth of the periodic structures. Results as a function of the pulse splitting are shown in Figure 4, where the value of the depth of the structures obtained under NPM irradiation is also indicated by the dashed horizontal line.

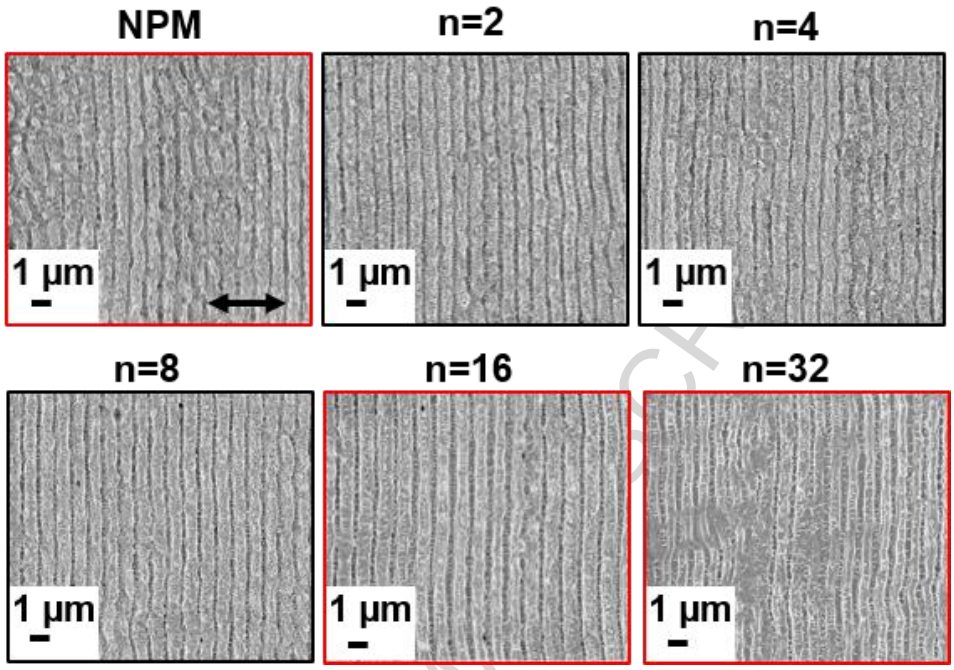

Fig. 3 – 1D-LIPSS obtained with bursts of variable number of pulses and intra-burst delay of 1.5 ps, with a fluence of 0.85 J/cm^2. The LIPSS obtained in NPM at the same total laser fluence are shown for comparison. The black double arrow indicates the direction of the incident polarization. Surfaces selected for wettability measurements are highlighted by red frames.

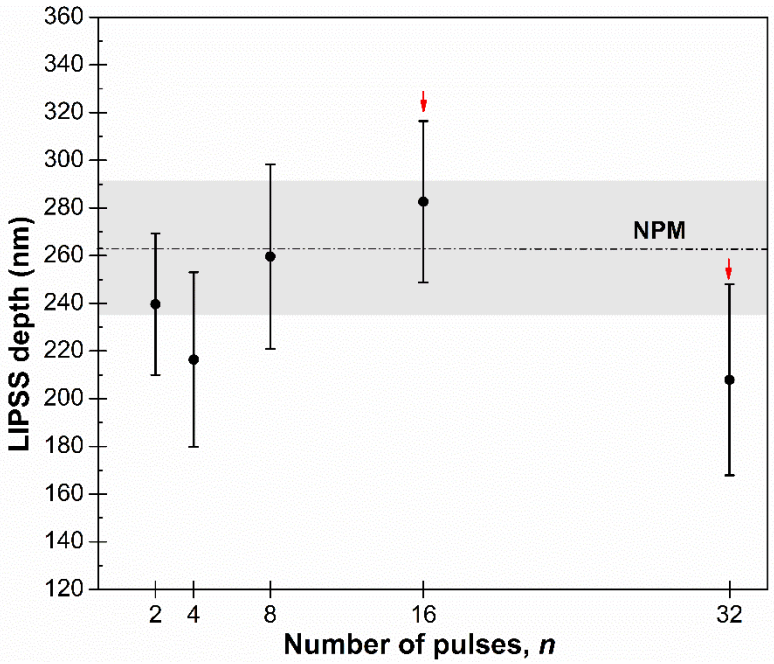

Fig. 4 - 1D-LIPSS depth as a function of the number of pulses in the bursts. The red arrows indicate the structures chosen for the wettability tests. The grey bar indicates the error bar related to depth measured in case of NPM irradiation.

Except for the case of n=16 sub-pulses, the LSFL produced under BM irradiation are generally slightly shallower than those obtained in NPM. It is worth noticing that, initially, the depth of the ripples increases with the number of sub-pulses in the burst, reaching its highest value for n=16. This is ascribable to incubation [38]. However, for n=32 the energy of each sub-pulse is significantly lower. In addition, for such a high number of sub-pulses, plasma shielding is supposed to reduce the laser energy hitting the surface. As a result, the ripples depth is considerably decreased for n=32 sub-pulses.
To study the effect of the 1D-LIPSS morphology on the surface wettability properties, we selected samples obtained with n=16 and n=32, as they showed ripples with highest and lowest depths, respectively d=283 nm for n=16 and d= 208 nm for n=32.

3.3 Surface structuring with circularly and cross polarized bursts

Figure 5 shows all the different types of surface textures that has been obtained using bursts of circularly (CP) or cross polarized (XP) sub-pulses, and varying the pulse splitting from n=2 to n=32 and the total laser fluence, while keeping the same intra-burst delay of 1.5 ps, scanning speed and hatch distance.

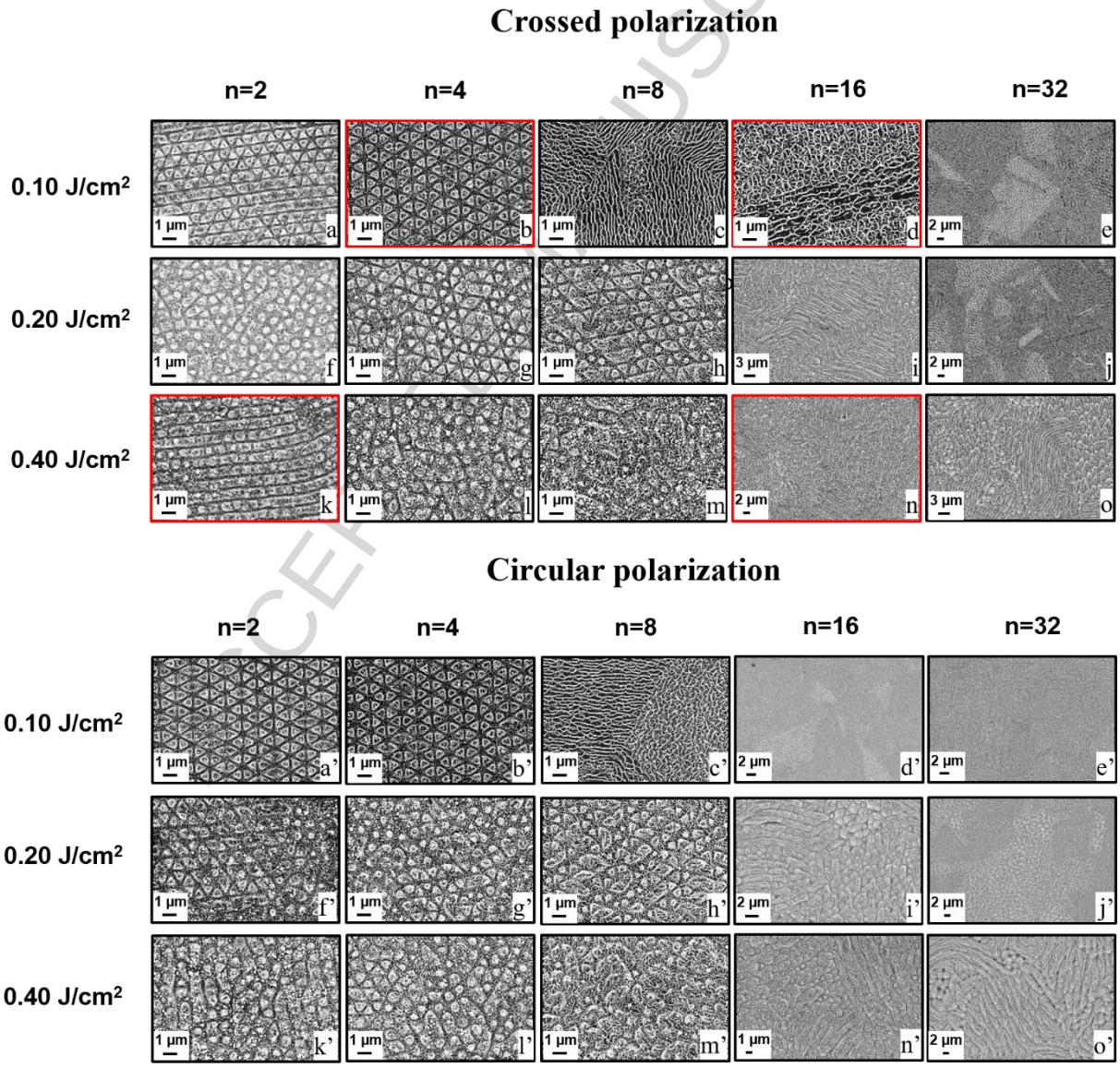

Fig. 5 - Evolution of structuring morphology with the variation of the number of pulses in the bursts and the total fluence. The time delay between pulses is fixed at 1.5 ps. Here, pps=20 and the hatch=2 µm.

Bi-dimensional texture patterns are formed whose morphology changes significantly according to the burst characteristics. No substantial difference is noticed between results of CP and XP bursts. At laser fluence values of 0.1 J/cm^2 and 0.2 J/cm^2 the triangular structures arranged in hexagonal lattice already observed with CP NPM (see Fig. 2e), are formed only for bursts with $2 \leq n \leq 8$. In this range of number of sub-pulses, the duration of each burst is between 1.5 ps and 10.5 ps. Similar results have been found in [30,31] where double pulses with crossed or circular polarization and comparable laser fluence were used. Here, the delay between the two pulses was systematically changed and the formation of the triangular structures was observed for intra-pulse delays of exactly the same timescale as in our results.

The formation of such structures can be attributed, in agreement with Bonse et al. [39], to interference effects between the incident light and a surface wave originated by the excitation of surface plasmon polaritons in a very early stage of the irradiation. This leads to a periodically modulated energy deposition and localized ablation. After the formation of the initial ripples, irradiation with multiple pulses triggers feedback mechanisms which lead to interference and consequent local field enhancement [40]. This hypothesis is also supported by Zhang et al. [41] who simulated the electric field distribution on a grooved surface finding that, after a certain amount of impinging femtosecond laser pulses, the electric field concentrates at the center of the grooves, thus determining1D or 2D periodic ablation patterns.

The polarization state of the incident laser radiation has also an influence on this inhomogeneous energy distribution. As a consequence, nanoripples or 1D-LIPSS are formed in case of irradiation with linearly polarized pulses while bi-dimensional periodic surface patterns are created with CP pulses or XP bursts, provided that the total burst duration is shorter than electron-phonon coupling. Indeed, as far as the number of sub-pulses in the bursts increases and thus the total burst duration gets longer, the linear LIPSS gets less homogeneous [27] and the triangular patterns disappear (Fig. 5). This happens probably because, at timescales longer than the electron-phonon coupling, thermal effects like expansion and melting of the lattice occur, thus changing the material absorption and reflectivity and, consequently, disturbing the interference mechanisms. Therefore, the most homogeneous and sharpest triangular structures are seen for bursts with n=2 or n=4 sub-pulses, while already for n=8 the structures appear shallower and less homogenous.

The laser fluence also plays an important role on the formation of the periodic surface patterns. In fact, at the higher fluence of 0.4 J/cm^2 the triangular structures do not form and disordered non-uniform structures are, instead, noticed both for CP and XP bursts irradiation (see Fig. 5k-m and Fig. 5k'-m'). This result is consistent with the previous explanation, since with the increase of the laser intensity the transition of the material from the solid to the molten state is facilitated. With the decomposition of the lattice, the coupling of the laser energy to the material is influenced and the energy deposition does not follow any more homogeneous patterns. Therefore, at the fluence of 0.4 J/cm^2 randomly distributed pillar-like structures are formed for $n \leq 8$ sub-pulses. For higher pulse splitting the pillars disappear and highly inhomogeneous bush-like structures are observed (see Fig. 5n-o and Fig. 5n'-o').

It is worth noticing that in NPM the process window to get the triangular structures is very narrow. When using bursts of pulses, the same type of structures can be generated in a wider range of laser fluence. In addition, by optimizing the polarization state of the burst, i.e. XP rather than CP, and the pulse splitting n=4, it is possible to generate very reproducible triangular structures with sharp edges homogenously distributed over large areas. A surface obtained with this combination of process parameters (see Fig. 5b) has been selected for the wettability measurements.

By further examining the images reported in Figure 4 of the surfaces produced with XP and CP bursts, it can be noted that for $n \geq 8$ sub-pulses and a fluence of 0.1 J/cm^2 a different type of surface structures appears, i.e. HSFL. Their orientation follows the polycrystalline nature of the substrate material, thus clearly unveiling the steel grain structure. This is due to the fact that when the pulse fluence is not sufficient to allow the generation of homogeneous LIPSS and fluences very close to the threshold are used, the formation of the HSFL strongly depends on the materials properties. Here, any inhomogeneity of the material like defects of the lattice or the different phases and orientations of the crystallographic structure affects the HSFL shape and orientation. Therefore, under particular irradiation conditions the grain structure is revealed [42]. In our case, only by using

bursts with a high number of XP or CP sub-pulses the crystallographic structure of the steel was highlighted, as it is better shown by the optical microscope image of Figure 6.

Fig. 6 - Optical microscope image of a target surface irradiated with bursts of 8 pulses with a time delay of 1.5 ps at a total fluence of 0.1 J/cm^2. The grain structure of the polycrystalline target is clearly visible.

This is very interesting for many applications since it shows that a laser surface treatment based on the use of bursts of femtosecond pulses may potentially replace traditional methods for the preparation of metallographic samples based on mechanical polishing and chemical etching.

3.4 Wetting behaviour

The wetting behavior of some representative structures was investigated. In particular, among the surfaces with 1D-LIPSS, the one obtained in NPM (indicated as 1D-LIPSS-NPM) and those produced in BM with the highest (1D-LIPSS-BM-n=16) and lowest (1D-LIPSS-BM-n=32) depths of the ripples have been chosen. Whereas for the 2D-LIPSS, the triangular, bush-like, pillar-like and HSFL following the crystallographic grains (2D-HSFL-grain) structures have been selected. All the selected structures are enclosed in red boxes in Figure 2 and in Figure 4. The wettability of a reference untreated (and as received) steel sample was also analyzed.
In the first column of Table 1, results of the static contact angles are presented for all the analyzed structures. These measurements were performed 55 days after the laser treatment, i.e. after that the wetting behavior had stabilized and the equilibrium angles (θ_{eq}) were reached, as will be explained in next sections. During this monitoring period the samples were stored in a laboratory environment in closed but not sealed boxes.

Table 1. Equilibrium static (θ_{eq}) and dynamic water contact angle measured on some representative laser textured surfaces. The values for the untreated steel surface are also reported.

Morphology	θ_{eq} (°)	θ_{eq}^{adv} (°)	θ_{eq}^{rec} (°)
1D-LIPSS-BM-n=16	160 ± 2	165 ± 2	27 ± 7
2D-LIPSS-Triangular	156 ± 1	157 ± 2	29 ± 6
1D-LIPSS-NPM	150 ± 2	158 ± 2	15 ± 1
1D-LIPSS-BM-n=32	139 ± 1	151 ± 1	20 ± 4
2D-HSFL-Grain	145 ± 2	151 ± 1	14 ± 1
2D-LIPSS-Bush	157 ± 1	158 ± 2	14 ± 3
2D-LIPSS-Pillar	124 ± 2	132 ± 3	25 ± 1

Un-treated (as received)	55 ± 2	67 ± 2	11 ± 3

As it can be clearly seen, at long-term air exposure after the laser treatment the surfaces are over-hydrophobic or even superhydrophobic (angle higher than 150°).
Similar results were also achieved on steel by [43] and [44] though under different conditions of the laser processing, i.e. wavelength of 1064 nm, 30 ns single pulses at 25 kHz and 800 nm, 150 fs at 1 kHz, respectively. Lower angles were instead found by [45] that achieved contact angles of up to 130° by irradiating a martensitic stainless steel sample with 800 nm, 125 fs single pulses at 5 kHz.
In the second and third column of table 1, the advancing and receding angles are respectively reported, also after the stabilization time. In all the laser treated cases, we find that the receding angle is very low; therefore, given the high advancing angles, a high angle hysteresis characterizes these surfaces. Generally, a high WCA hysteresis indicates that the surface is highly adhesive towards water drops [46,47]. This effect is ascribed to either topographical or chemical heterogeneities, thus it can be found on smooth as well as textured surfaces. In the case of textured hydrophobic and superhydrophobic surfaces, such a high adhesion to the liquid indicates that a total or partial Wenzel regime is established, hence a full or quasi-full contact between water and solid exists (i.e. air pockets are absent or unstable) [48].
As it will be clearer in next sections, the water adhesive character is mostly due to the specific chemical composition of this surface.
The time variation of the static contact angle after the treatment and until equilibrium was also investigated. This specific study was conducted, by weekly measuring the angle on replica samples, for two different structures, namely the 1D LIPSS- BM – n=16 and 2D LIPSS – Triangular.

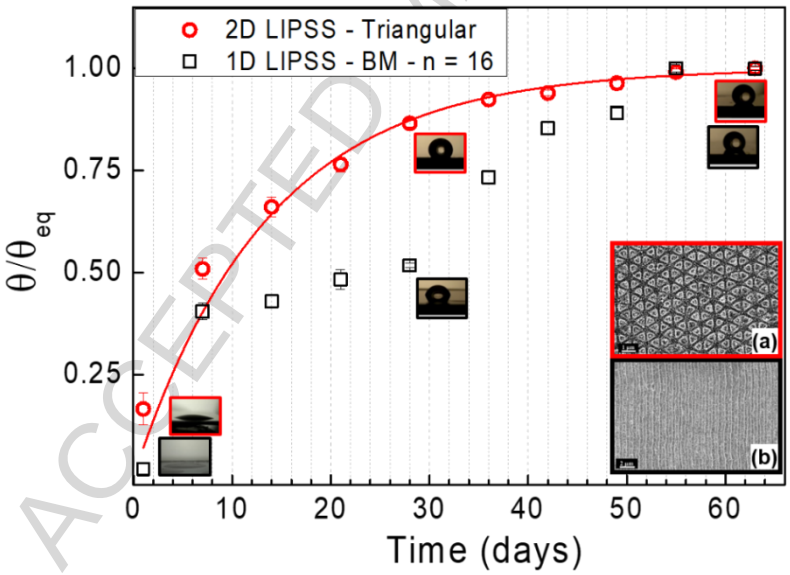

Fig. 7 – Time dependence of the contact angle for the 1D-LIPSS with n=16 pulses (black open square) and for the 2D-LIPSS (red open circle).

The laser treated surfaces showed an initial hydrophilic /super-hydrophilic behaviour, characterized by contact angles equal to 3° ± 2° (superhydrophilic when lower than 5°) and 26° ± 6° (markedly hydrophilic) for 1D-LIPSS and 2D-LIPSS with triangular structure, respectively. These values are sensitively smaller than that of the non-treated surface, indicating that the laser treatment leads, soon after the process, to an activation of the metal surface towards the contact with polar compounds and specifically water.
As shown by the diagram in Figure 7, for both the investigated morphologies, the increase of the contact angle is fairly exponential in agreement with literature about laser [44] or plasma

treatments [49]. The exponential growth appears particularly neat for the triangular laser modified surface.
Thus, in this case a fitting has been operated by using the law:

$$\frac{\theta}{\theta eq} = 1 - e^{-\frac{t}{\lambda}}$$

With θeq being the already mentioned steady state (equilibrium) water contact angle and λ the constant characteristic for the growth (at which the angle is the 63% of the final one). For such a surface λ equals 13.6 days.
We observe that this parameter is relatively high (i.e. the angle growth is relatively slow) with respect to other laser processed steel surfaces in literature [43–45]. In particular, Kietzig et al. [44] showed the variation of this parameter as a function of the irradiation conditions and the alloy composition. Reasonably, also the environmental/exposure conditions (temperature, humidity, aeration conditions) must have a role in the velocity of the aging process [50].
The linear surface structures (1D LIPSS – BM n=16) instead, show over time a less monotonous increase. This has been reported under several conditions of the laser process investigated by [43] and in some materials investigated by Kietzig [44], too.
At the equilibrium time both surfaces turned out super-hydrophobic, reaching contact angle values of 160° ± 2° and 157° ± 3°, for 1D-LIPSS and 2D-LIPSS with triangular structure, respectively.

3.5 Surface chemistry evolution

XPS survey spectra are reported in Figure 5 to have a view at a glance of the variation first induced by the laser treatment, then by the long-term interaction with the atmosphere. In Table 2 atomic XPS % of C, O, Fe, Cr are reported for the untreated and the treated 1D-LIPSS and 2D-LIPSS with triangular structure, at one day (fresh) and at two months after the treatment (aged), with the samples stored in closed not sealed boxes in the laboratory air environment. It was found that 2 months after the treatment, a steady surface energy condition was reached, as seen above.

Table 2. XPS atomic % for untreated and laser treated steel samples subjected to aging investigation. Atomic ratios for O/Fe and C/Fe

Surface	C(%)	O(%)	Fe(%)	Cr(%)	O/Fe	C/Fe
Untreated	74	23	2.2	0.8	10.4	34
2D- LIPSS Triangular fresh	22	46	27	5	1.7	0.8
1D-LIPSS BM n=16 fresh	20	48	22	10	2.2	0.9
2D- LIPSS Triangular aged	51	34	10	5	3.4	5.1
1D-LIPSS BM n=16 aged	56	32	8	4	4	7

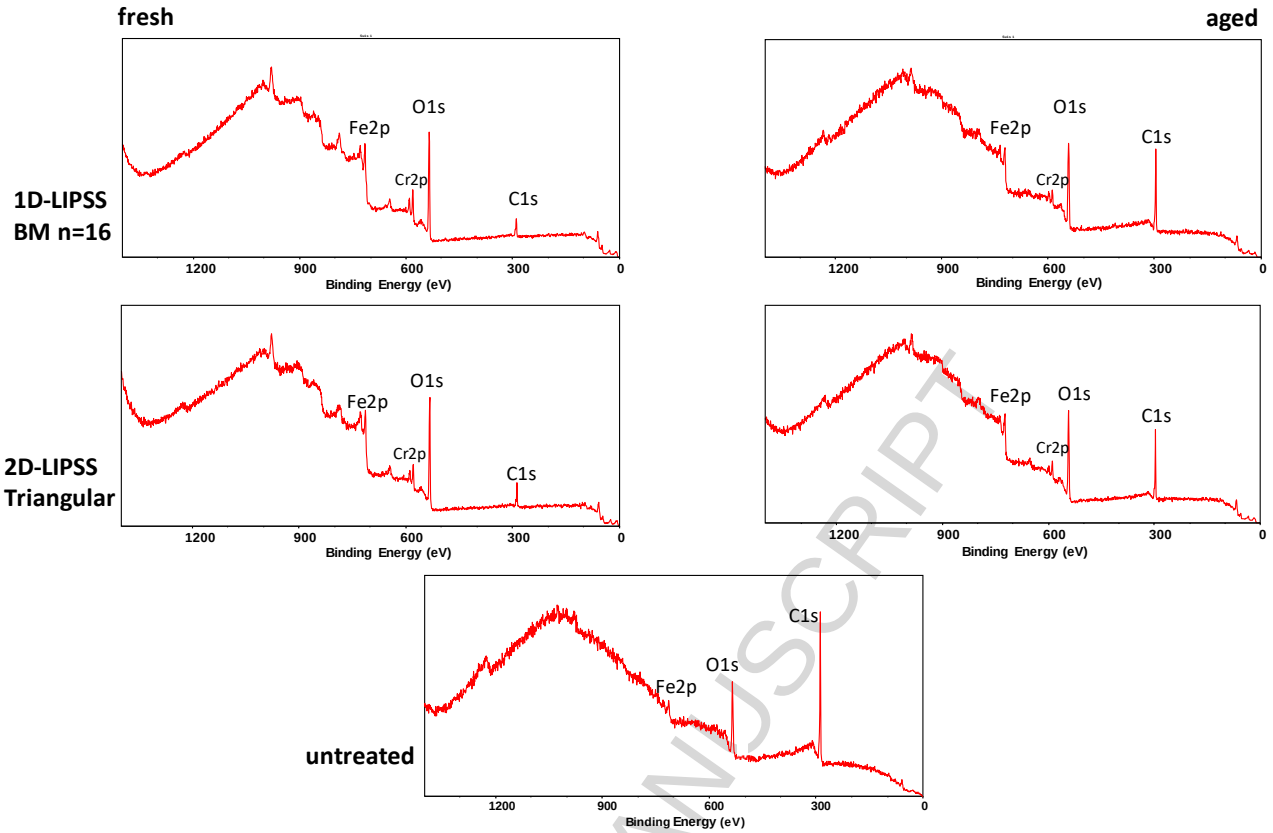

Fig. 8 - Survey XPS spectra for untreated, and 1D-LIPSS – BM – n=16 and 2D-LIPSS triangular laser textured steel surfaces, at 1 day (fresh) and 2 months after the treatment.

The untreated steel surface is characterized by very high atomic % of carbon, lower % of oxygen, and extremely low % of metals Fe and Cr (Ni was fairly detectable but hardly quantified). This sample, as above reported, was not cleaned before the analysis, and was instead analyzed just after the removal of the plastic protective film. This was the same condition at which the laser treatment was performed and the WCA measurement was conducted.
On the freshly treated surfaces a steep reduction of the surface C content is observed, thing which can be ascribed to the effectiveness of the laser treatment in removing the adventitious carbon contamination from the surface. Meanwhile, Fe and Cr increase importantly, while the O increase, though sensitive, appears less pronounced; the C/Fe and O/Fe ratios, reported in the same table, decrease with the former showing the most drastic decrease.
These indirect data, i.e the C/Fe and O/Fe ratios, describe the variation of the surface chemical state since C and O are spy elements more involved in the interaction between the surface and the environment, such as the adsorption/chemisorption of hydrocarbons and the oxidation reactions with oxygen and the moistures present in the atmosphere.
As it can be derived from Table 2, upon aging the C/Fe and O/Fe ratios increase again, but without restoring the same levels of the untreated surface.
Figure 9 shows the normalized high resolution C1s spectra curve-fitted with a SLG(30) peak shape. The components are reported, together with the corresponding area %, in table 3: C0 (carbide C, 283.8 ± 0.2 eV), C1 (C-C(H) 284.8 ± 0.3 eV), C2 (C-O, 286.3 ±0.3 eV), C3 (C(O)O, 288±0.3 eV). C1, C2 and C3 are typically associated to adventitious carbon for high resolution C1s deconvoluted peak [51].
Freshly treated surfaces, where the C1s signal is less intense (% in Table 2), have higher oxygenated components, i.e. C2 and C3, which, instead, appear reduced upon aging. This means that over the aging time, while the carbon total % increases (Table 2) the relative content of carbon-oxygen species/groups gets lower with respect to the total carbon, reasonably as a consequence of the progressive enrichment of non-oxygen-bonded hydrocarbon species/groups

(C1 component). A similar effect had been already shown in [52] for hydrophilic treated plastic materials.
Interestingly, upon aging, an important difference is present on the linear aged samples where a splitting of the C1 component is observed with the appearance of a new one, termed C0, which being at lower BE than the C-C(H), is necessarily to be ascribed to carbide carbon atoms, i.e. bonded with a metal, such as Fe or Cr. This can be considered an evidence of the peculiar reactivity of this treated surface with the environment atmosphere.
Figure 10 reports the normalized Fe2p (3/2, ½) XPS spectra of the same surfaces, where the positions of the major components are indicated (Fe metal, 707 eV; Fe (II) oxide, 709.5 eV; Fe (III) oxide,711eV). The higher noise on the untreated specimen signal is due to its very low intensity in the as acquired (not normalized) spectrum (low metal % in untreated surface). For both these treatments, it is possible to observe that the freshly treated surfaces have distinguishable contributions of Fe(metal) and Fe(II) oxide components, which are then reduced upon aging. This confirms the capability of the treatment in removing the outermost, more oxidized layers of the material (cleaning action). This effect is lost over time since the metal evolves towards more oxidized forms. That is why we have highlighted that during exposure time, though the O % decreases, the O/Fe increases.

Table 3 - Area % of the components used in the best fitting procedure of the C1s high resolution XPS signal for untreated and laser treated steel samples subjected to aging investigation.

	C0 (area %)	**C1 (area %)**	**C2 (area %)**	**C3 (area %)**
Untreated	-	77	14	9.2
2D-LIPSS-Triangular fresh	-	65.6	20.5	13.7
2D-LIPSS-Triangular aged	-	84.4	7.6	8
1D-LIPSS-BM-n=16 fresh	-	57.1	22.9	19.9
1D-LIPSS-BM-n=16aged	46.4	39.1	7.2	7.2

However, the Fe metallic component is particularly pronounced only on the 1D-LIPSS surface, where it can be assumed that a more energetic cleaning of the steel surface has taken place since the fluence of the sub-pulses (defined as the fluence of the burst divided by the number of sub-pulses within the burst) was double (0.05 J/cm^2) compared to the 2D-LIPSS case (0.025 J/cm^2). This effect probably can explain the different reactivity of this surface, on which the exposition to atmosphere leads to the appearance of carbide carbon moieties at long-term (Fig.9). To this effect should be also ascribed the irregular increase of the contact angle over time shown by this surface (diagram in Figure 7), where, likely, various reactive paths take place which have different velocities and variously contribute to the global change of the surface energy over time.
As a concluding consideration, we find that over the time after the treatment within the outermost surface layer (the one which is sampled by XPS) the principal effects are the following: i) the total carbon percentage increases and becomes richer in hydrocarbons and poorer in oxygen-bonded carbon species; ii) metals decrease in atomic percentage but becomes more oxidized.
In literature it had been noted that a correlation exists between the final total carbon content and the (static) angle of equilibrium θ_{eq} [44]. Actually this is what we also find, as above reported. However, deeper insights can be gained from the chemical and wetting characterization. The final chemical configuration of the surface includes a high amount of carbon as hydrocarbon (or carbide in some cases) with still a significant content of metals in highly oxidized form. From the wetting point of view, this implies a mixed hydrophobic (hydrocarbons) and hydrophilic (in general all the carbon-oxygen bonds and in particular the C(O)O groups, the Me-Me and Me-O bonds)

configuration. This heterogeneity explains the high hysteresis found in aged surfaces, hence their high water-adhesive, though superhydrophobic, behavior. As previously commented about the dynamic angle measurements, the advancing CA is more sensitive to low-energy components of the surface, while the receding angle is more sensitive to the high-energy ones [47].
Indeed, it can be reasonably thought that the water front moving on these surfaces after a first unfavorable contact with the surface, as revealed by the high advancing angle, finds out chemical domains where a high affinity exists and from which to recede is unfavorable (hence the receding angle is very low).
The fact that the advancing/static angle are so high, indicates that the roughness/texture induced by the treatment is suitable to get a superhydrophobic behavior.

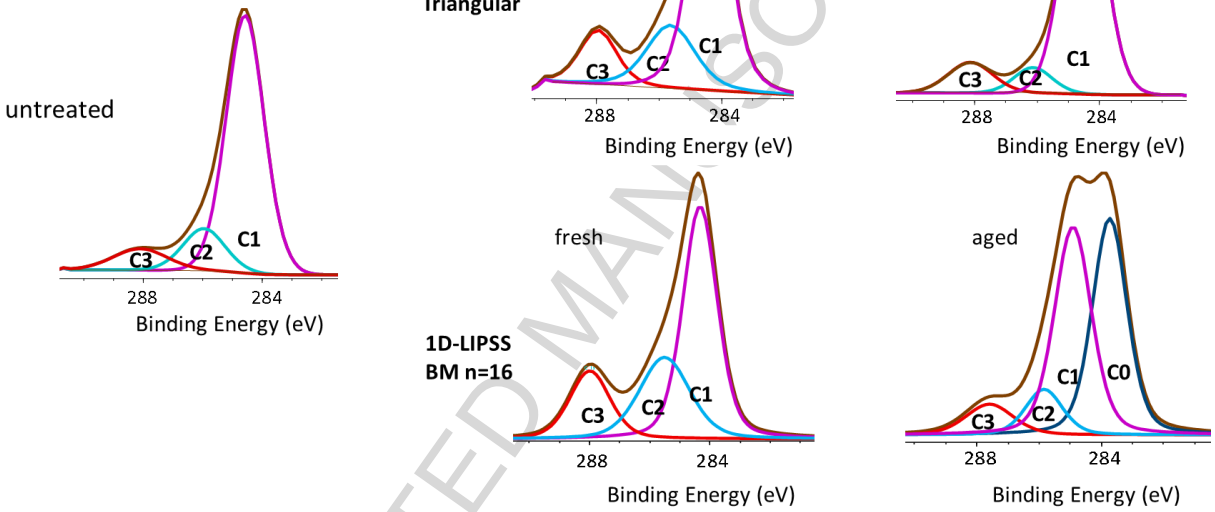

Fig. 9 - Normalised high resolution C1s XPS spectra for untreated, 1D-LIPSS n=16 and 2D-LIPSS triangular laser textured steel surfaces, at 1 day (fresh) and 2 months after the treatment.

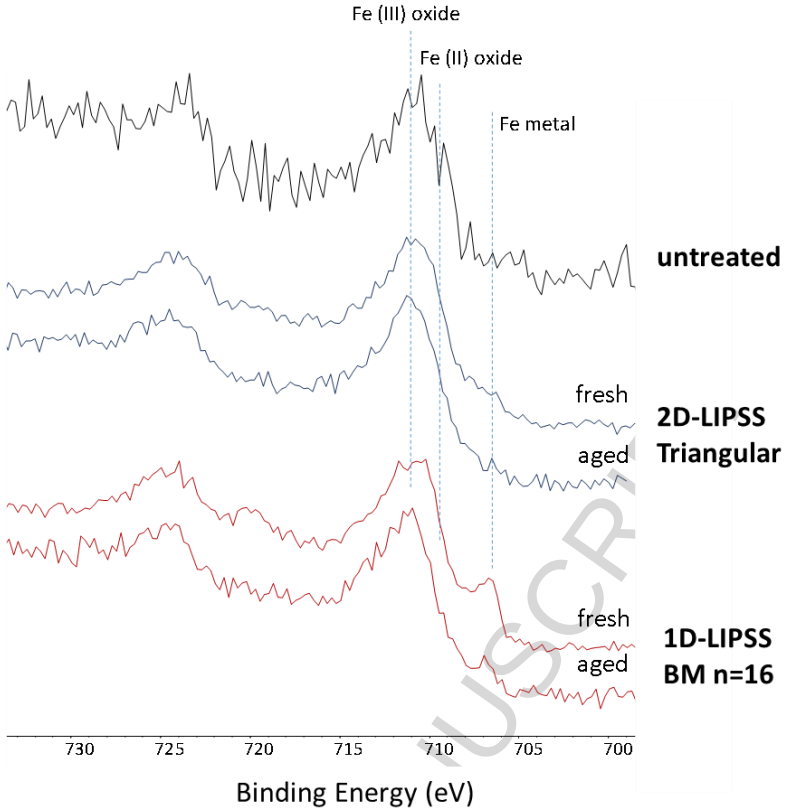

Fig. 10 - Normalised high resolution Fe2p XPS spectra for untreated, 1D-LIPSS n=16 and 2D-LIPSS triangular laser textured steel surfaces, at 1 day (fresh) and 2 months after the treatment.

4. Conclusions

The interplay between surface chemistry and morphology has been investigated on the short and long term wetting behavior of stainless steel surfaces laser textured, respectively, with bursts of femtosecond pulses and in normal pulse mode (i.e. no burst).
It was found that the morphology of the surface textures changes significantly depending on the laser irradiation parameters. In Normal Pulse Mode, linearly polarized pulses produce 1D periodic structures, which are classified, respectively, as high spatial frequency LIPSS for high values of accumulated laser fluence and low spatial frequency LIPSS for lower fluences. When using circularly polarized pulses and accumulated fluence of 24 J/cm^2, 2D regular patterns of triangular structures arranged over hexagons were obtained, whereas at higher accumulated fluences non-periodic pillar-like patterns were generated. Working with bursts of pulses with fixed intra-burst delay of 1.5 ps allowed producing different surface topographies by changing the number of pulses in the burst and their polarization state, besides the accumulated laser fluence. This could be easily done by exploiting the extreme flexibility of the burst generator setup consisting of a cascade of rotating birefringent crystals. Linearly polarized bursts enabled to produce 1D-LIPSS with the possibility to change the depth of the ripples by adjusting the number of pulses in the burst. Circular and crossed polarized bursts allowed generating a wide range of patterns: 2D highly regular patterns of triangular structures, HSFL oriented along the grains of the polycrystalline material, and non-periodic structures such as micro-bushes or micro-pillars. It is worth noting that the triangular structures were obtained both in NPM as well as in BM. However, in BM the process window to generate such structures was significantly wider, as far as the total duration of the bursts employed was shorter than the electron-phonon coupling, in good agreement with [30]. The physical mechanisms behind the formation of the triangular periodic patterns are still not fully understood but further investigating such mechanisms was beyond the scope of the present work. However, our results indicate that the formation of highly regular 2D-LIPSS occurs before the electron-phonon coupling time, which is compatible with the hypothesis, supported by many

authors, that the underlying mechanism is the interference between the incident light and excited surface plasmon polaritons [39,41]. Indeed, for longer bursts it has been shown here that such 2D patterns disappear, probably due to thermal effects, like melting and lattice decomposition which typically occur on a time scale longer than the electron-phonon coupling.

The long term wetting behavior of seven selected laser textured samples characterized by quite different 1D and 2D surface topographies was investigated. All the morphologies showed hydrophobicity or super-hydrophobicity, with static contact angles varying from 124° to 160°, while the dynamic measurements exhibited high hysteresis thus indicating adhesive behavior. To further understand this result, the temporal evolution of the contact angle was investigated for the two surfaces showing the highest hydrophobicity. Starting from an initial hydrophilic state, immediately after the laser treatment, an increase of the contact angle with time was found following an exponential law. The surface chemistry XPS analyses indicated that the laser treatment initially removes the adventitious carbon contamination, with varying degrees of cleaning extents depending on the sub-pulse laser fluence, which explains the hydrophilic behavior. During exposure to the ambient atmosphere, the surfaces become richer in hydrocarbons (or carbide in some cases) and poorer in oxygen-bonded species, while metal species on the surfaces decrease in atomic percentage but become more oxidized. While the former effect is noteworthy correlated with the increase of the advancing/static angle (increase of the hydrophobic character), the latter is considered responsible of the rather low receding angles, hence of the water adhesive character of these surfaces. Such surface chemistry heterogeneity explains the high dynamic contact angle hysteresis and, hence, the surfaces high water-adhesive, though superhydrophobic, behavior. The surface topography is assumed to play a role especially in connection with the high advancing/static angle, which indicates that the roughness/texture induced by the laser treatment hinders the water-solid contact. However, in the few contact domains, the high surface chemistry affinity makes the receding less favorable.

We highlight that the water adhesiveness and superhydrophobicity (very high advancing and static angle) of such surfaces allow indicating the no loss droplet reversible transportation as suited application [42,43]. Applications as self-cleaning, anti-icing are certainly possible with these specific surfaces, once a proper homogeneously hydrophobic chemical modification (coating, treatment,) is accomplished.

Acknowledgements

The authors would like to gratefully thank Pietro Paolo Calabrese for his technical support.

References

[1] M. Birnbaum, Semiconductor surface damage produced by Ruby lasers, J. Appl. Phys. 36 (1965) 3688–3689. doi:10.1063/1.1703071.

[2] J. Bonse, S. Hohm, S. V. Kirner, A. Rosenfeld, J. Kruger, Laser-Induced Periodic Surface Structures-A Scientific Evergreen, IEEE J. Sel. Top. Quantum Electron. 23 (2017). doi:10.1109/JSTQE.2016.2614183.

[3] X. Sedao, A. Abou Saleh, A. Rudenko, T. Douillard, C. Esnouf, S. Reynaud, C. Maurice, F. Pigeon, F. Garrelie, J.P. Colombier, Self-Arranged Periodic Nanovoids by Ultrafast Laser-Induced Near-Field Enhancement, ACS Photonics. 5 (2018) 1418–1426. doi:10.1021/acsphotonics.7b01438.

[4] N.A. Kirichenko, E. V. Barmina, G.A. Shafeev, Theoretical and Experimental Investigation of the Formation of High Spatial Frequency Periodic Structures on Metal Surfaces Irradiated by Ultrashort Laser Pulses, Phys. Wave Phenom. 26 (2018) 264–273. doi:10.3103/S1541308X18040027.

[5] O. Varlamova, K. Hoefner, M. Ratzke, J. Reif, D. Sarker, Modification of surface properties of solids by femtosecond LIPSS writing: comparative studies on silicon and stainless steel, Appl. Phys. A Mater. Sci. Process. 123 (2017) 0. doi:10.1007/s00339-017-1362-y.

[6] S. Gräf, F.A. Müller, Polarisation-dependent generation of fs-laser induced periodic surface structures, Appl. Surf. Sci. 331 (2015) 150–155. doi:10.1016/j.apsusc.2015.01.056.

[7] R. Sugawara, S. Sekiguchi, T. Yagi, Formation of periodic ripples through excitation of ~1 μm spot using femtosecond-laser Bessel beam on c-Si, Appl. Surf. Sci. 353 (2015) 400–404. doi:10.1016/j.apsusc.2015.06.108.
[8] G.F.B. Almeida, R.J. Martins, A.J.G. Otuka, J.P. Siqueira, C.R. Mendonca, Laser induced periodic surface structuring on Si by temporal shaped femtosecond pulses, Opt. Express. 23 (2015) 27597. doi:10.1364/OE.23.027597.
[9] J. Heitz, B. Reisinger, M. Fahrner, C. Romanin, J. Siegel, V. Svorcik, Laser-induced periodic surface structures (LIPSS) on polymer surfaces, Int. Conf. Transparent Opt. Networks. (2012) 1–4. doi:10.1109/ICTON.2012.6253723.
[10] E. Rebollar, M. Castillejo, T.A. Ezquerra, Laser induced periodic surface structures on polymer films: From fundamentals to applications, Eur. Polym. J. 73 (2015) 162–174. doi:10.1016/j.eurpolymj.2015.10.012.
[11] M. Martínez-Calderon, M. Manso-Silván, A. Rodríguez, M. Gómez-Aranzadi, J.P. García-Ruiz, S.M. Olaizola, R.J. Martín-Palma, Surface micro- and nano-texturing of stainless steel by femtosecond laser for the control of cell migration, Sci. Rep. 6 (2016) 1–10. doi:10.1038/srep36296.
[12] E. Rebollar, I. Frischauf, M. Olbrich, T. Peterbauer, S. Hering, J. Preiner, P. Hinterdorfer, C. Romanin, J. Heitz, Proliferation of aligned mammalian cells on laser-nanostructured polystyrene, Biomaterials. 29 (2008) 1796–1806. doi:10.1016/j.biomaterials.2007.12.039.
[13] Z. Wang, Q. Zhao, C. Wang, Reduction of friction of metals using laser-induced periodic surface nanostructures, Micromachines. 6 (2015) 1606–1616. doi:10.3390/mi6111444.
[14] Z. Ou, M. Huang, F. Zhao, The fluence threshold of femtosecond laser blackening of metals: The effect of laser-induced ripples, Opt. Laser Technol. 79 (2016) 79–87. doi:10.1016/j.optlastec.2015.11.018.
[15] G. Li, J. Li, Y. Hu, C. Zhang, X. Li, J. Chu, W. Huang, Femtosecond laser color marking stainless steel surface with different wavelengths, Appl. Phys. A Mater. Sci. Process. 118 (2014) 1189–1196. doi:10.1007/s00339-014-8868-3.
[16] S. Razi, O. Varlamova, J. Reif, M. Bestehorn, S. Varlamov, M. Mollabashi, K. Madanipour, M. Ratzke, Birth of periodic Micro/Nano structures on 316L stainless steel surface following femtosecond laser irradiation; single and multi scanning study, Opt. Laser Technol. 104 (2018) 8–16. doi:10.1016/j.optlastec.2018.02.001.
[17] E. Allahyari, J. JJ Nivas, S.L. Oscurato, M. Salvatore, G. Ausanio, A. Vecchione, R. Fittipaldi, P. Maddalena, R. Bruzzese, S. Amoruso, Laser surface texturing of copper and variation of the wetting response with the laser pulse fluence, Appl. Surf. Sci. 470 (2019) 817–824. doi:10.1016/j.apsusc.2018.11.202.
[18] Z. Yang, C. Zhu, N. Zheng, D. Le, J. Zhou, Superhydrophobic Surface Preparation and Wettability Transition of Titanium Alloy with Micro/Nano Hierarchical Texture, Materials (Basel). 11 (2018) 2210. doi:10.3390/ma11112210.
[19] P. Gregorčič, M. Sedlaček, B. Podgornik, J. Reif, Formation of laser-induced periodic surface structures (LIPSS) on tool steel by multiple picosecond laser pulses of different polarizations, Appl. Surf. Sci. 387 (2016) 698–706. doi:10.1016/j.apsusc.2016.06.174.
[20] A.M. Bonch-Bruevich, Surface electromagnetic waves in optics, Opt. Eng. 31 (1992) 718. doi:10.1117/12.56133.
[21] G. Li, J. Li, X. Li, Z. Zhu, Y. Hu, J. Chu, W. Huang, Evolution of titanium surfaces irradiated by femtosecond laser pulses with different wavelengths, 8769 (2013) 87691V. doi:10.1117/12.2021098.
[22] P. Nürnberger, H. Reinhardt, H.C. Kim, F. Yang, K. Peppler, J. Janek, N. Hampp, Influence of substrate microcrystallinity on the orientation of laser-induced periodic surface structures, J. Appl. Phys. 118 (2015). doi:10.1063/1.4932215.
[23] E.M. Hsu, T.H.R. Crawford, H.F. Tiedje, H.K. Haugen, Periodic surface structures on gallium phosphide after irradiation with 150 fs-7 ns laser pulses at 800 nm, Appl. Phys. Lett. 91 (2007) 2005–2008. doi:10.1063/1.2779914.
[24] J. Bonse, S. Höhm, A. Rosenfeld, J. Krüger, Sub-100-nm laser-induced periodic surface structures upon irradiation of titanium by Ti:sapphire femtosecond laser pulses in air, Appl. Phys. A Mater. Sci. Process. 110 (2013) 547–551. doi:10.1007/s00339-012-7140-y.
[25] K. Okamuro, M. Hashida, Y. Miyasaka, Y. Ikuta, S. Tokita, S. Sakabe, Laser fluence

dependence of periodic grating structures formed on metal surfaces under femtosecond laser pulse irradiation, Phys. Rev. B - Condens. Matter Mater. Phys. 82 (2010) 1–5. doi:10.1103/PhysRevB.82.165417.

[26] J.J.J.N. Ivas, F.G. Esuele, E.A. Llahyari, S.L.O. Scurato, R.F. Ittipaldi, A. V Ecchione, R.B. Ruzzese, S.A. Moruso, Effects of ambient air pressure on surface structures produced by ultrashort laser pulse irradiation, 42 (2017) 2710–2713.

[27] G. Giannuzzi, C. Gaudiuso, C. Di Franco, G. Scamarcio, P.M. Lugarà, A. Ancona, Large area laser-induced periodic surface structures on steel by bursts of femtosecond pulses with picosecond delays, Opt. Lasers Eng. 114 (2019) 15–21. doi:10.1016/j.optlaseng.2018.10.006.

[28] J. Romano, A. Garcia-giron, P. Penchev, S. Dimov, Triangular laser-induced submicron textures for functionalising stainless steel surfaces, Appl. Surf. Sci. 440 (2018) 162–169. doi:10.1016/j.apsusc.2018.01.086.

[29] Q.I.L. Iu, N.A.N.Z. Hang, J.I.Y. Ang, H.O.Q. Iao, C.H.G. Uo, Direct fabricating large-area nanotriangle structure arrays on tungsten surface by nonlinear lithography of two femtosecond laser beams, 26 (2018) 11718–11727.

[30] F. Fraggelakis, G. Mincuzzi, J. Lopez, I. Manek-hönninger, R. Kling, Applied Surface Science Controlling 2D laser nano structuring over large area with double femtosecond pulses, Appl. Surf. Sci. 470 (2019) 677–686. doi:10.1016/j.apsusc.2018.11.106.

[31] F. Fraggelakis, G. Giannuzzi, C. Gaudiuso, I. Manek-Hönninger, G. Mincuzzi, A. Ancona, R. Kling, Double- and Multi-Femtosecond Pulses Produced by Birefringent Crystals for the Generation of 2D Laser-Induced Structures on a Stainless Steel Surface, Materials (Basel). 12 (2019) 1257. doi:10.3390/ma12081257.

[32] S. Rung, S. Schwarz, B. Götzendorfer, C. Esen, R. Hellmann, Time Dependence of Wetting Behavior Upon Applying Hierarchic Nano-Micro Periodic Surface Structures on Brass Using Ultra Short Laser Pulses, Appl. Sci. 8 (2018) 700. doi:10.3390/app8050700.

[33] D. Huerta-Murillo, A. García-Girón, J.M. Romano, J.T. Cardoso, F. Cordovilla, M. Walker, S.S. Dimov, J.L. Ocaña, Wettability modification of laser-fabricated hierarchical surface structures in Ti-6Al-4V titanium alloy, Appl. Surf. Sci. 463 (2019) 838–846. doi:10.1016/j.apsusc.2018.09.012.

[34] S. Zhou, D. Ouzounov, H. Li, I. Bazarov, B. Dunham, C. Sinclair, F.W. Wise, Efficient temporal shaping of ultrashort pulses with birefringent crystals, (2007) 2–6.

[35] B. Dromey, M. Zepf, M. Landreman, K.O. Keeffe, T. Robinson, S.M. Hooker, Generation of a train of ultrashort pulses from a compact birefringent crystal array, (2007) 1–5.

[36] F. Fraggelakis, G. Mincuzzi, J. Lopez, I. Manek-Hönninger, R. Kling, Texturing metal surface with MHz ultra-short laser pulses, Opt. Express. 25 (2017) 18131. doi:10.1364/OE.25.018131.

[37] J. Romano, A. Garcia-giron, P. Penchev, S. Dimov, Applied Surface Science Triangular laser-induced submicron textures for functionalising stainless steel surfaces Ultra short pulsed ShuΣer laser source Quarter Waveplate 100mm F- θ lens Scanning Δz, Appl. Surf. Sci. 440 (2018) 162–169. doi:10.1016/j.apsusc.2018.01.086.

[38] C. Gaudiuso, G. Giannuzzi, A. Volpe, P.M. Lugarà, I. Choquet, A. Ancona, Incubation during laser ablation with bursts of femtosecond pulses with picosecond delays, Opt. Express. 26 (2018) 3801. doi:10.1364/OE.26.003801.

[39] J. Bonse, A. Rosenfeld, J. Krüger, On the role of surface plasmon polaritons in the formation of laser-induced periodic surface structures upon irradiation of silicon by femtosecond-laser pulses, J. Appl. Phys. 106 (2009). doi:10.1063/1.3261734.

[40] J. Bonse, S. Baudach, J. Krüger, W. Kautek, M. Lenzner, Femtosecond laser ablation of silicon-modification thresholds and morphology, Appl. Phys. A Mater. Sci. Process. 74 (2002) 19–25. doi:10.1007/s003390100893.

[41] C.-Y. Zhang, J.-W. Yao, H.-Y. Liu, Q.-F. Dai, L.-J. Wu, S. Lan, V.A. Trofimov, T.M. Lysak, Colorizing silicon surface with regular nanohole arrays induced by femtosecond laser pulses, Opt. Lett. 37 (2012) 1106. doi:10.1364/OL.37.001106.

[42] X. Sedao, C. Maurice, F. Garrelie, J. Colombier, S. Reynaud, R. Quey, Influence of crystal orientation on the formation of femtosecond laser-induced periodic surface structures and lattice defects accumulation Influence of crystal orientation on the formation of femtosecond

laser-induced periodic surface structures and latt, 171605 (2014). doi:10.1063/1.4874626.
[43] M.H. Gregorčič, P., Marjetka Conradi, Luka Hribar, Long-Term Influence of Laser-Processing Parameters on (Super) hydrophobicity Development and Stability, Materials (Basel). 11 (2018). doi:10.3390/ma11112240.
[44] A.-M. Kietzig, S.G. Hatzikiriakos, P. Englezos, Patterned Superhydrophobic Metallic Surfaces, Langmuir. 25 (2009) 4821–4827. doi:10.1021/la8037582.
[45] P. Bizi-bandoki, S. Valette, E. Audouard, S. Benayoun, Applied Surface Science Time dependency of the hydrophilicity and hydrophobicity of metallic alloys subjected to femtosecond laser irradiations, Appl. Surf. Sci. 273 (2013) 399–407. doi:10.1016/j.apsusc.2013.02.054.
[46] C.G.. Furmidge, Studies at phase interfaces. I. The sliding of liquid drops on solid surfaces and a theory for spray retention, J. Colloid Sci. 17 (1962) 309–324. doi:https://doi.org/10.1016/0095-8522(62)90011-9.
[47] R. Di Mundo, F. Palumbo, Comments Regarding 'An Essay on Contact Angle Measurements,' Plasma Process. Polym. 8 (2011) 14–18. doi:10.1002/ppap.201000090.
[48] A.-M. Kietzig, M.N. Mirvakili, S. Kamal, P. Englezos, S.G. Hatzikiriakos, Laser-Patterned Super-Hydrophobic Pure Metallic Substrates: Cassie to Wenzel Wetting Transitions, J. Adhes. Sci. Technol. 25 (2011) 2789–2809. doi:10.1163/016942410X549988.
[49] B.R. Strohmeier, Improving the wettability of aluminum foil with oxygen plasma treatments, J. Adhes. Sci. Technol. 6 (1992) 703–718. doi:10.1163/156856192X01051.
[50] G.G. Cameron, Polymer surfaces: from physics to technology. F. Garbassi, M. Morra and E. Ochiello. John Wiley and Sons, Chichester, 1994. pp. ix+462, price £60.00. ISBN 0-471-93817-3, Polym. Int. 36 (1995) 300. doi:10.1002/pi.1995.210360314.
[51] /xpssimplified.com, (n.d.). https://xpssimplified.com/elements/carbon.php.
[52] R. Di Mundo, R. d'Agostino, F. Palumbo, Long-Lasting Antifog Plasma Modification of Transparent Plastics, ACS Appl. Mater. Interfaces. 6 (2014) 17059–17066. doi:10.1021/am504668s.

Graphical abstract

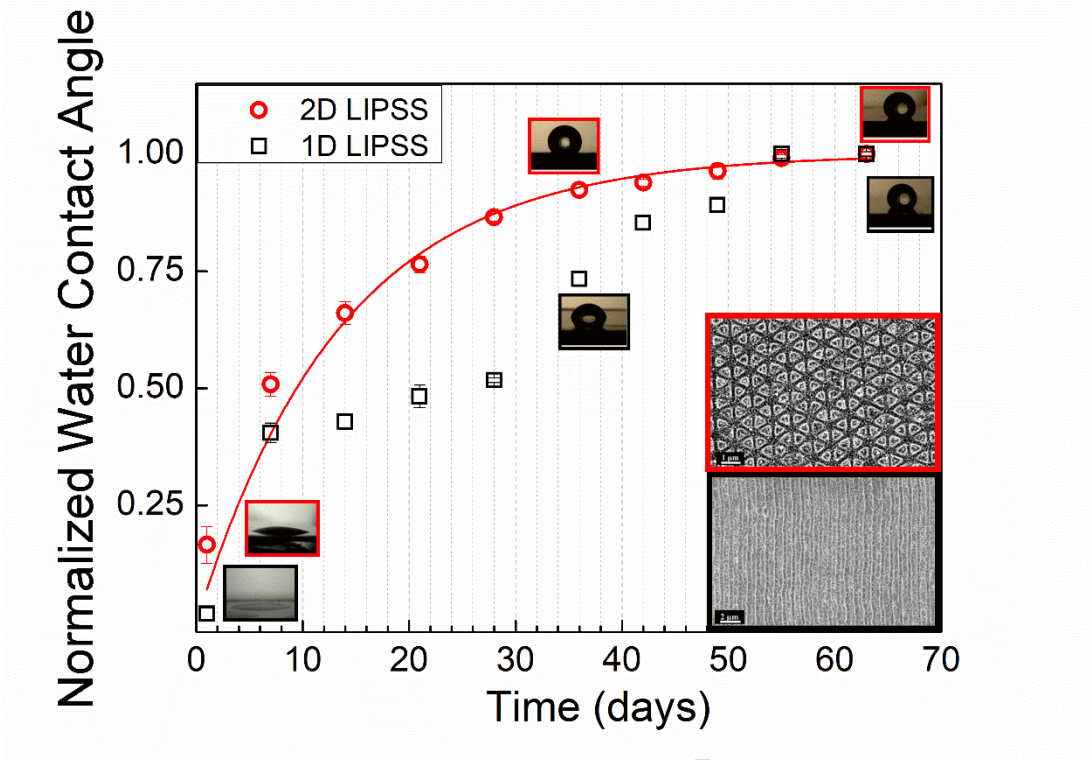

Time dependence of the contact angle for the 1D-LIPSS obtained with bursts of n=16, linearly polarized pulses (black open square) and for the 2D-LIPSS obtained with bursts of n=4, crossed polarized pulses (red open circle). The time delay in both cases is 1.5 ps.

Highlights

- 1D-LIPSS with variable period were obtained with bursts of linearly polarized pulses with ps intraburst delay
- 2D-LIPSS (triangles arranged over hexagons) were produced with bursts of crossed and circular polarization
- Changing the number of pulses within the bursts allowed varying the morphology of surface structuring among several patterns
- The contact angle of the laser treated surfaces varied over the time, settling at values close to 160° at long term with high hysteresis
- Over the exposure time the laser treated steel surfaces become richer in hydrocarbons and present more oxidized metals

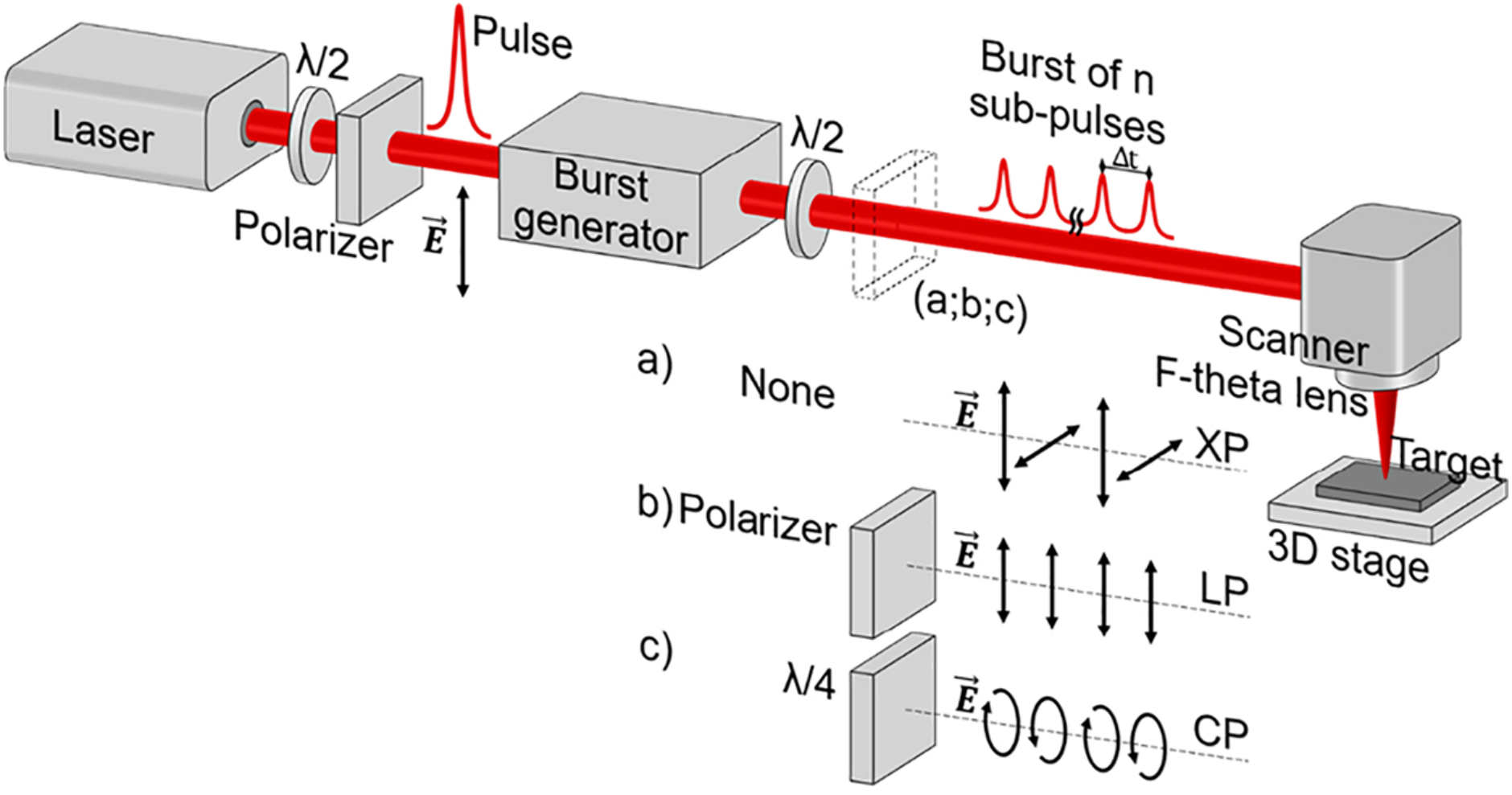
Laser
λ/2
Polarizer
$\vec{E}$
Pulse
Burst generator
λ/2
Burst of n sub-pulses
Δt
(a;b;c)
Scanner
F-theta lens
Target
3D stage
a) None
$\vec{E}$
XP
b) Polarizer
$\vec{E}$
LP
c) λ/4
$\vec{E}$
CP

Figure 1

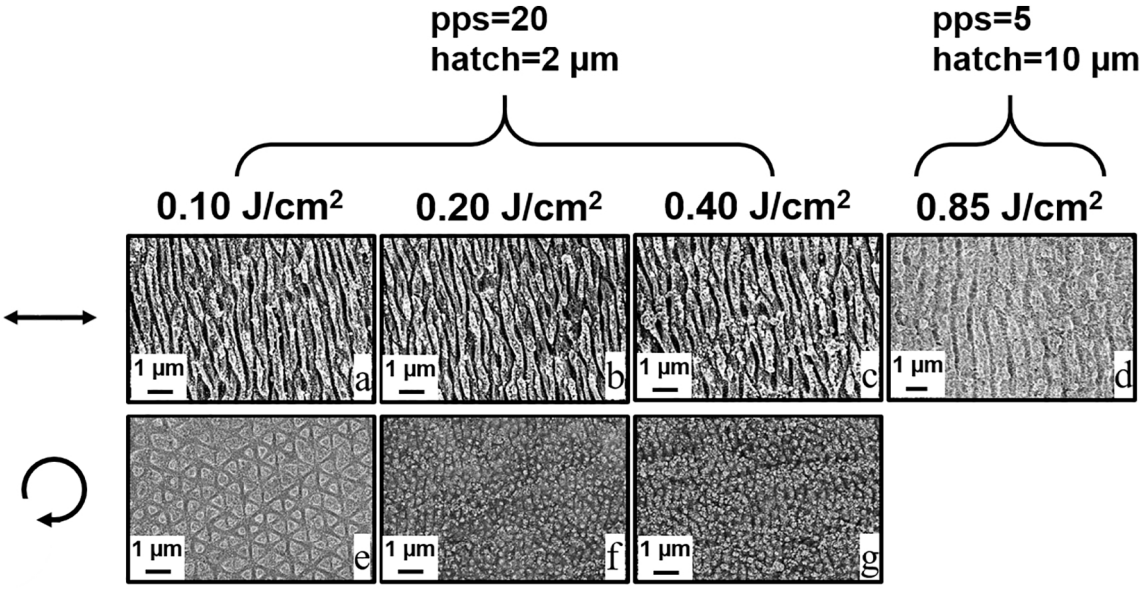
pps=20
hatch=2 µm
pps=5
hatch=10 µm
0.10 J/cm²
0.20 J/cm²
0.40 J/cm²
0.85 J/cm²
1 µm
a
1 µm
b
1 µm
c
1 µm
d
1 µm
e
1 µm
f
1 µm
g

Figure 2

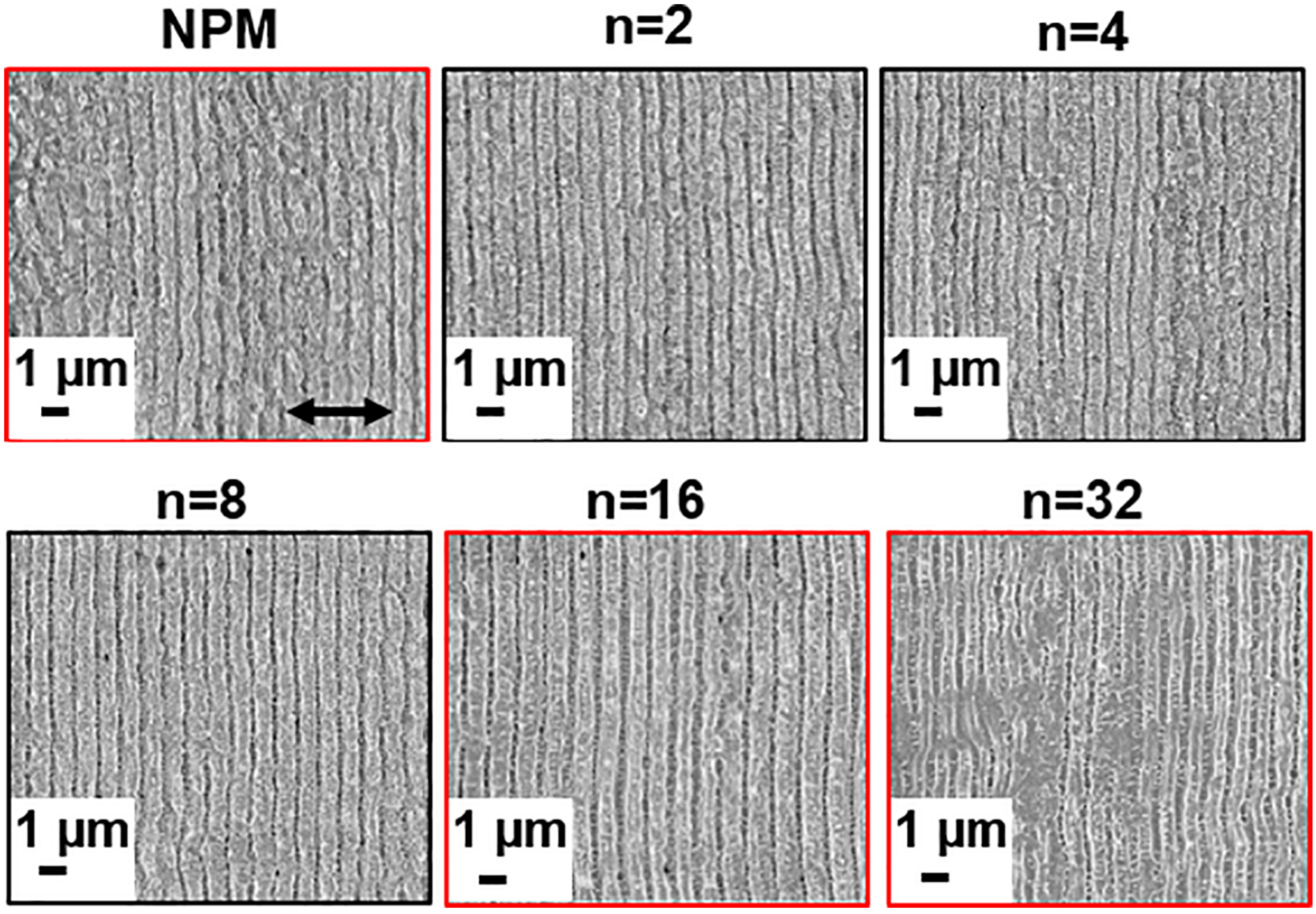

Figure 3

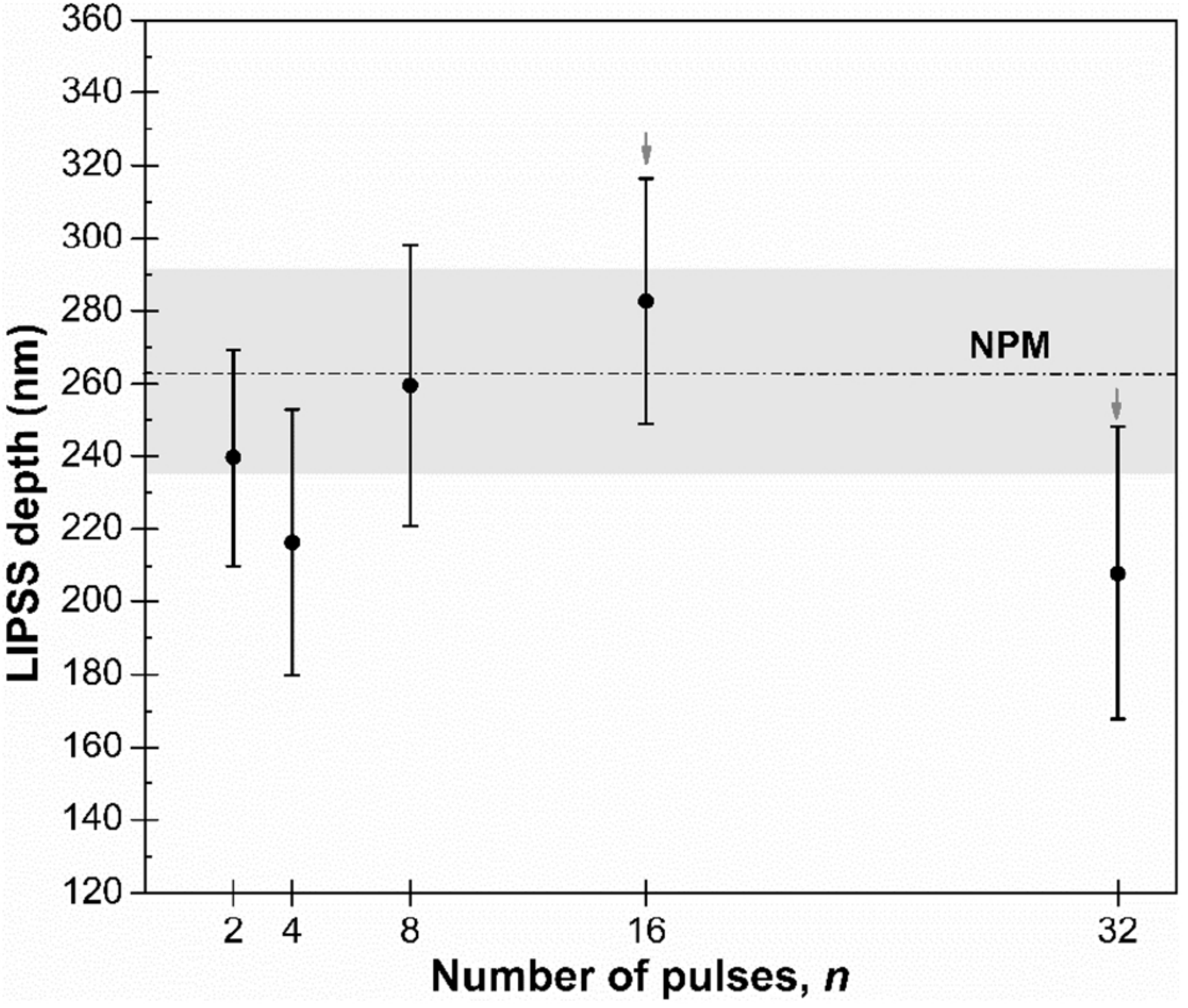
360
340
320
300
280
260
240
220
200
180
160
140
120
LIPSS depth (nm)
NPM
2
4
8
16
32
Number of pulses, n

Figure 4

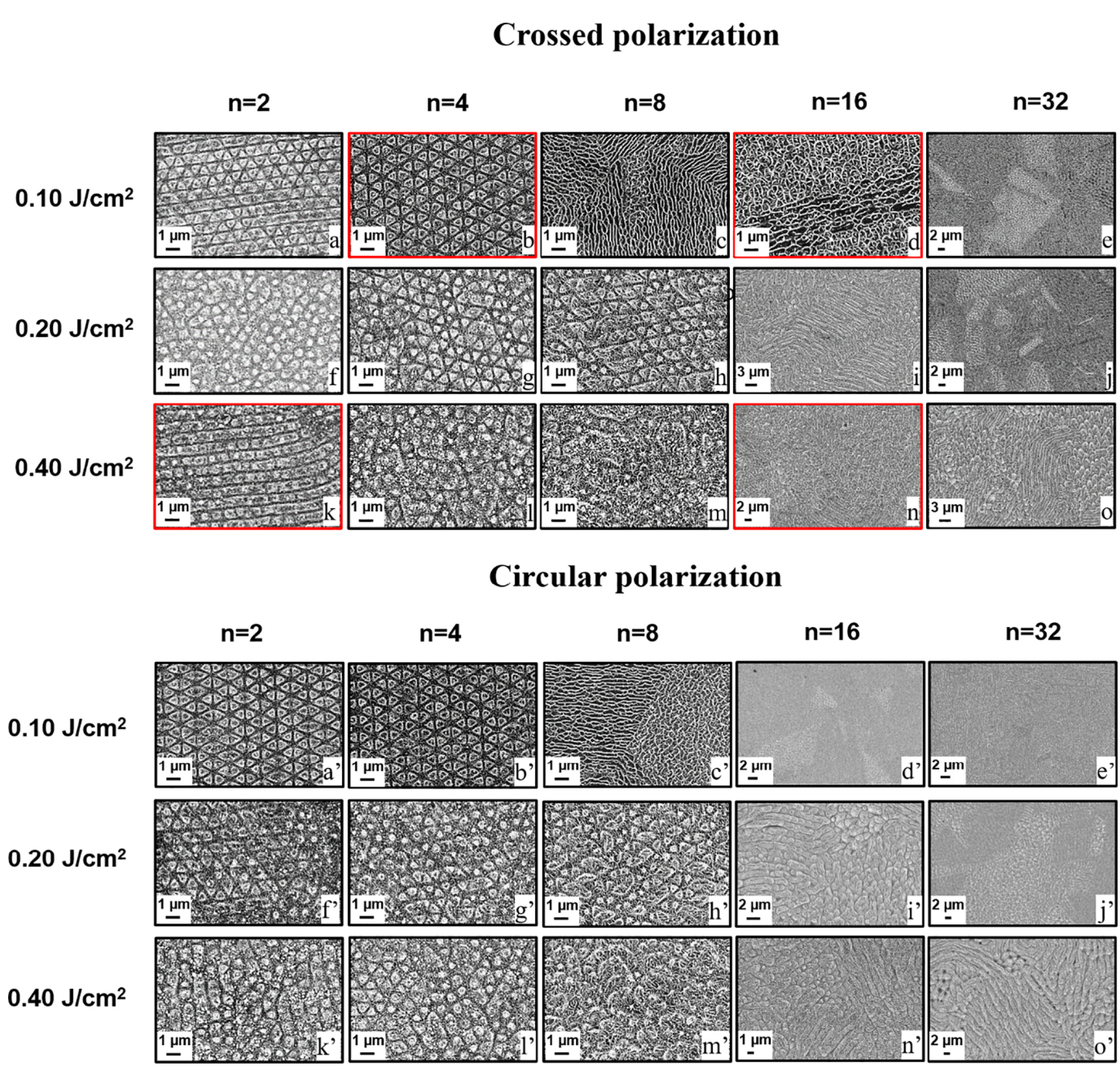
Crossed polarization
n=2
n=4
n=8
n=16
n=32
0.10 J/cm²
0.20 J/cm²
0.40 J/cm²
1 μm
2 μm
3 μm
a
b
c
d
e
f
g
h
i
j
k
l
m
n
o
Circular polarization
n=2
n=4
n=8
n=16
n=32
0.10 J/cm²
0.20 J/cm²
0.40 J/cm²
1 μm
2 μm
a'
b'
c'
d'
e'
f'
g'
h'
i'
j'
k'
l'
m'
n'
o'

Figure 5

Figure 6

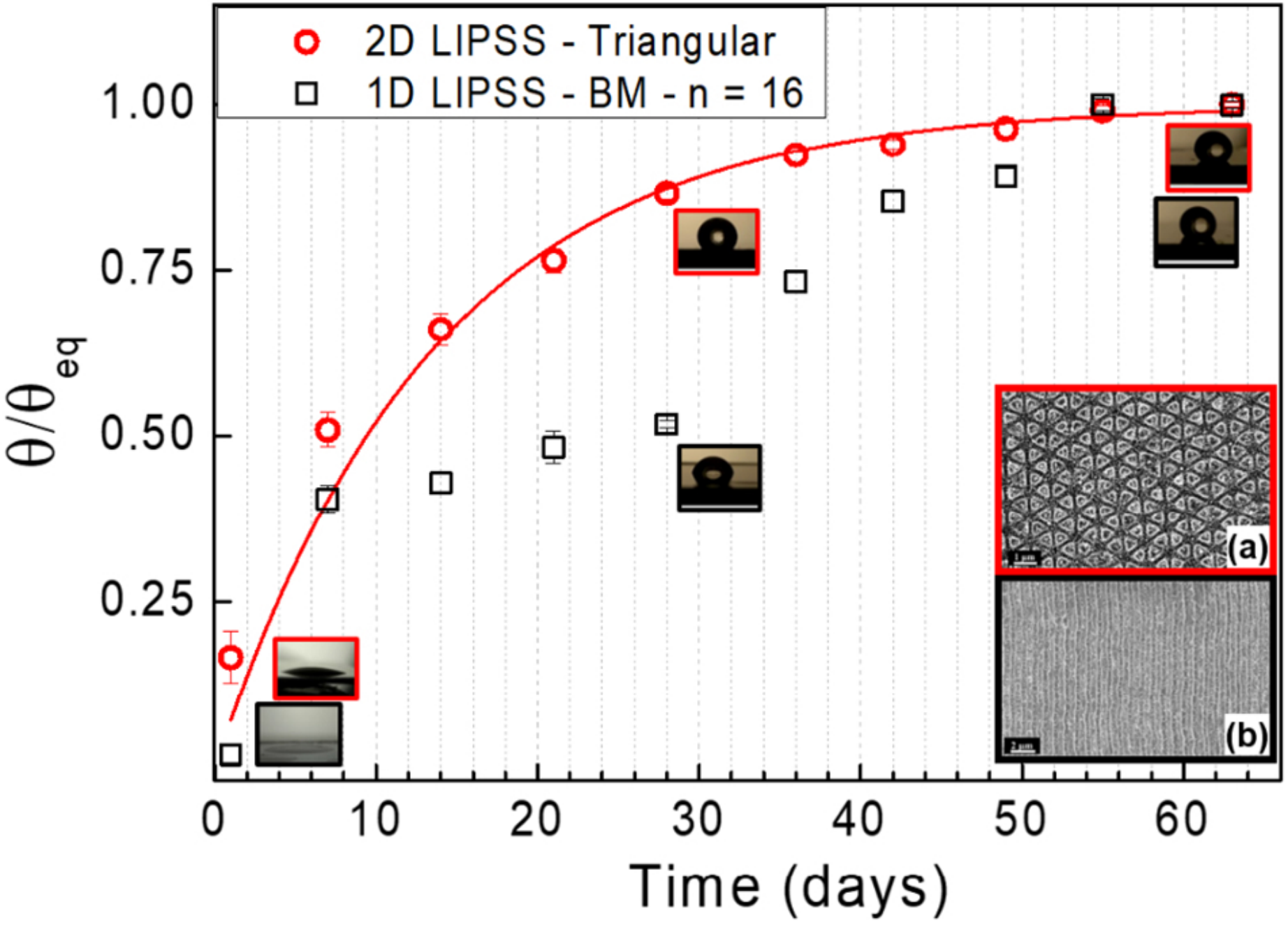
2D LIPSS - Triangular
1D LIPSS - BM - n = 16
1.00
0.75
0.50
0.25
θ/θeq
0
10
20
30
40
50
60
Time (days)
(a)
(b)

Figure 7

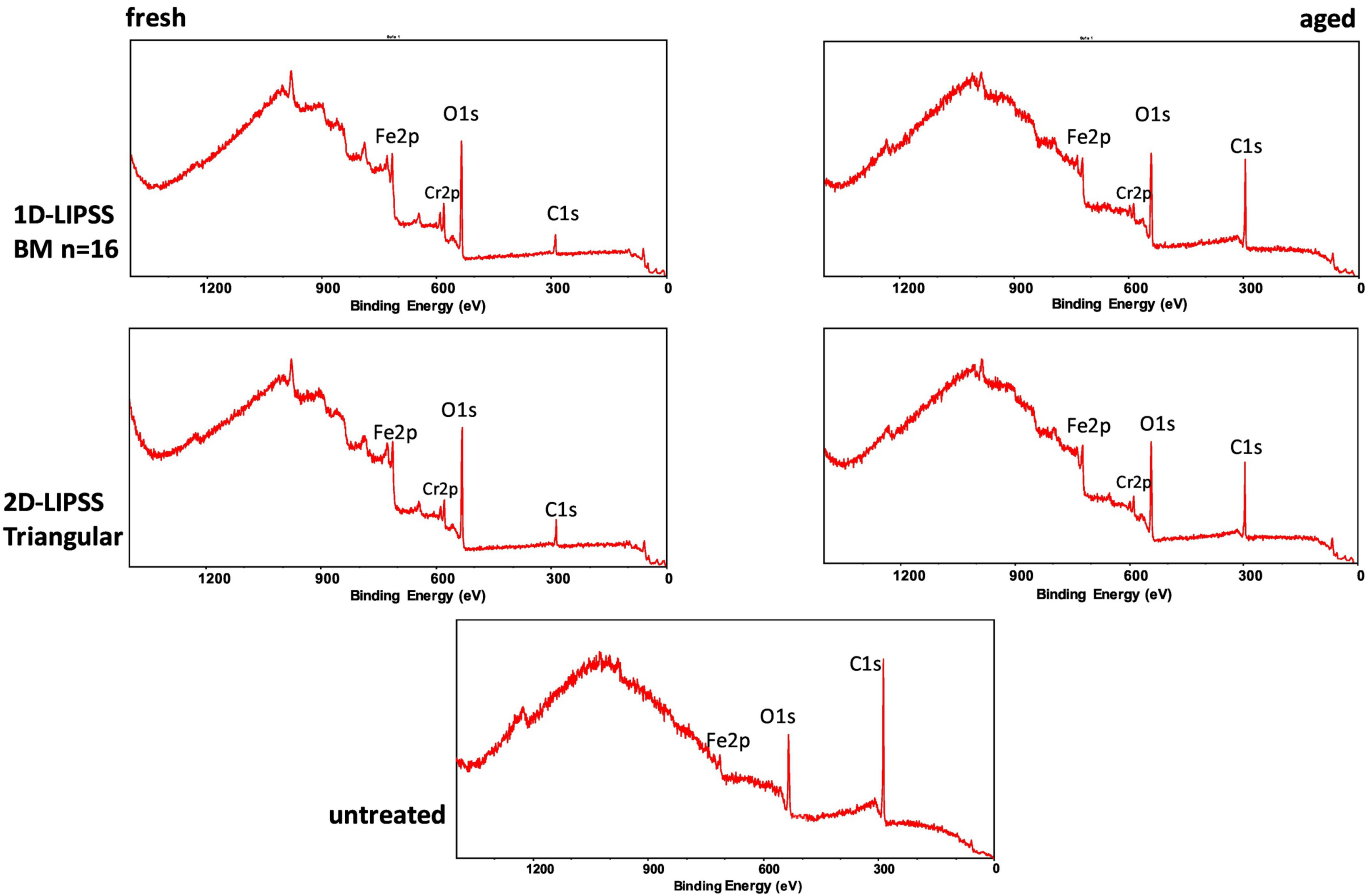
fresh
aged
1D-LIPSS
BM n=16
2D-LIPSS
Triangular
untreated
Fe2p
O1s
Cr2p
C1s
1200
900
600
300
0
Binding Energy (eV)

Figure 8

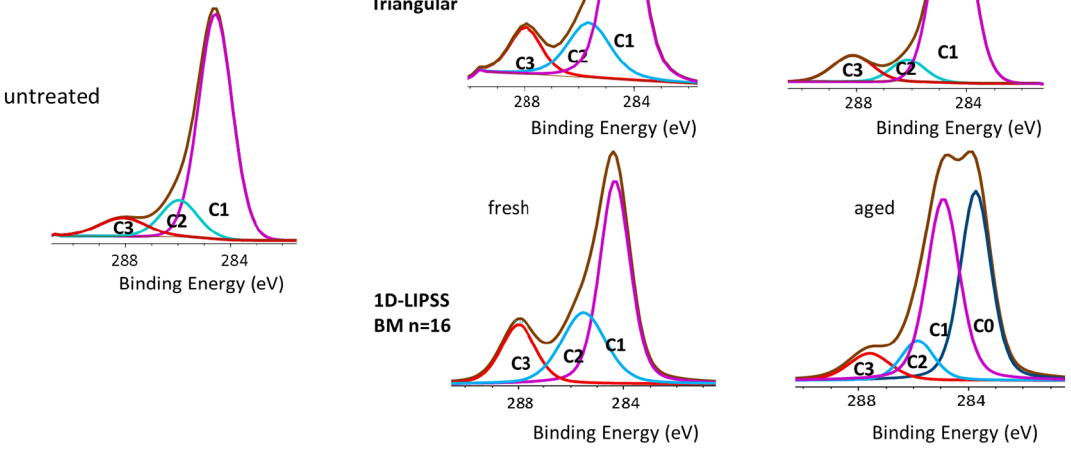
untreated
C3
C2
C1
288
284
Binding Energy (eV)
2D-LIPSS
Triangular
fresh
C3
C2
C1
288
284
Binding Energy (eV)
aged
C3
C2
C1
288
284
Binding Energy (eV)
1D-LIPSS
BM n=16
fresh
C3
C2
C1
288
284
Binding Energy (eV)
aged
C3
C2
C1
C0
288
284
Binding Energy (eV)

Figure 9

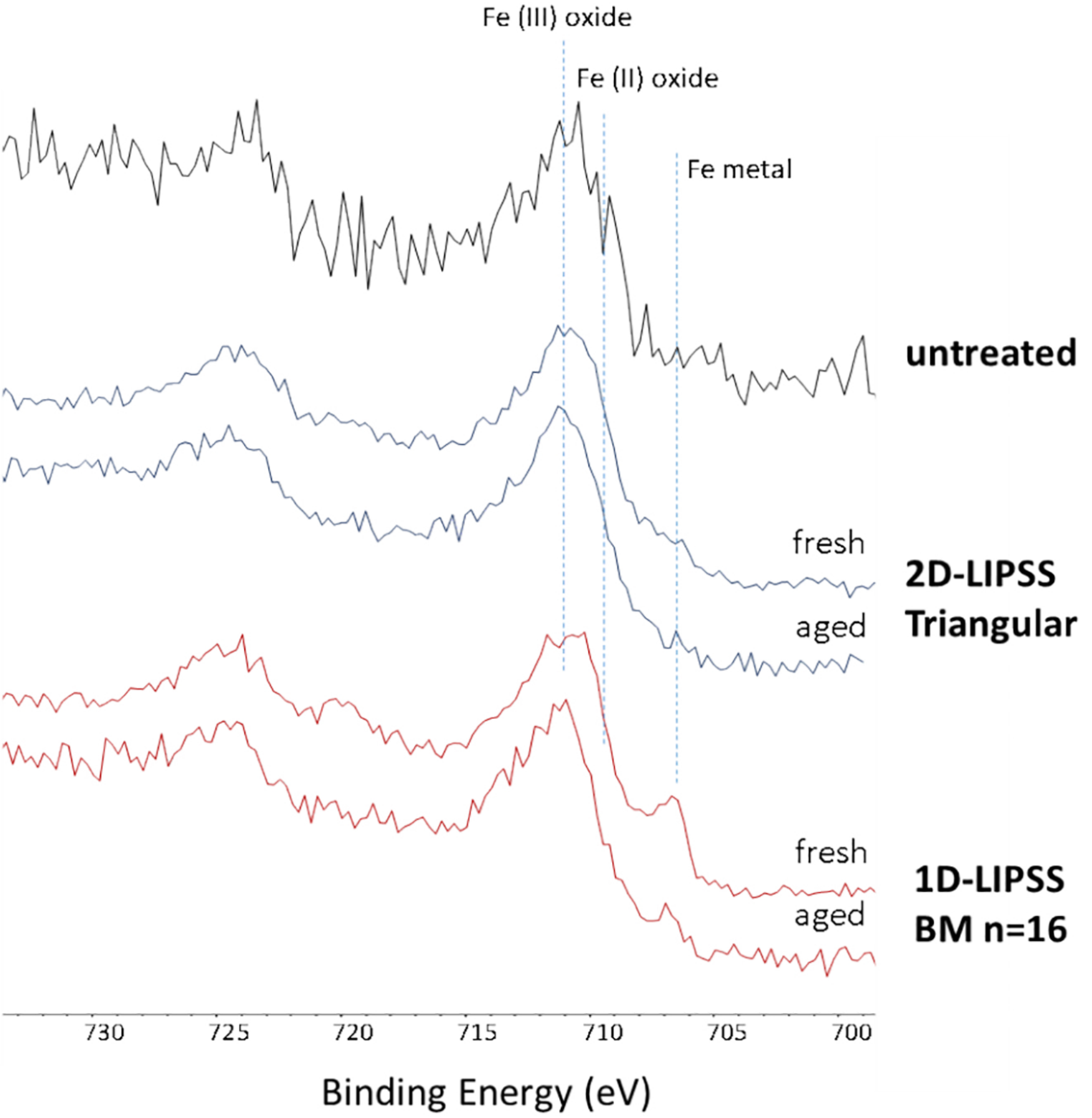
Fe (III) oxide
Fe (II) oxide
Fe metal
untreated
fresh
aged
2D-LIPSS
Triangular
fresh
aged
1D-LIPSS
BM n=16
730
725
720
715
710
705
700
Binding Energy (eV)

Figure 10